Gondwana Research 27 (2015) 594–611

Contents lists available at ScienceDirect

Gondwana Research

journal homepage: www.elsevier.com/locate/gr

Depletion and refertilization of the Tethyan oceanic upper mantle as revealed by the early Jurassic Refahiye ophiolite, NE Anatolia—Turkey

Ibrahim Uysal [a,*], E. Yalçın Ersoy [b], Yildirim Dilek [c], Monica Escayola [d], Ender Sarıfakıoğlu [e], Samet Saka [a], Takafumi Hirata [f]

[a] Department of Geological Engineering, Karadeniz Technical University, TR-61080 Trabzon, Turkey
[b] Department of Geological Engineering, Dokuz Eylül University, TR-35160 Izmir, Turkey
[c] Department of Geology & Environmental Earth Science, Miami University, Oxford, OH, 45056, USA
[d] Universidad Nacional de Salta, Buenos Aires 117, 4400 Salta, Argentina
[e] General Directorate of MTA, Geological Research Department, 06520 Ankara, Turkey
[f] Department of Geology and Mineralogy, Graduate School of Science, Kyoto University, Kitashirakawa Oiwakecho, Sakyo-ku, Kyoto 606-8502, Japan

ARTICLE INFO

Article history:
Received 26 April 2013
Received in revised form 6 September 2013
Accepted 7 September 2013
Available online 7 October 2013

Keywords:
Neotetyhan ophiolite
HSE and Re–Os isotope geochemistry
U–Pb zircon dating
Mantle refertilization
Partial melting of upper mantle

ABSTRACT

We present new whole-rock major and trace element, Re–Os isotope and mineral chemistry data for the upper mantle peridotites and mafic rocks in the Rehafiye ophiolite in NE Anatolia (Turkey), and discuss their significance for the mantle evolution in Neotethys. The Refahiye peridotites include clinopyroxene (cpx)-rich and cpx-poor harzburgites. Assuming an initial fertile mantle composition, the cpx-rich harzburgites have a limited range of Cr-spl Cr# (33–38), implying 14–18% melt extraction. However, TiO_2 contents of the Cr-spl in these rocks are too high (up to 0.24 wt.%) to explain their Ti concentrations with a simple melt extraction model in a mid-ocean ridge (MOR) setting, and suggest re-crystallization from an impregnating fertile melt. The interstitial phases of cpx in these samples have high TiO_2 (up to 0.40 wt.%) and Na_2O (up to 0.25 wt.%) contents. They also contain interstitial pargasitic amphibole with TiO_2 contents varying between 0.69 and 0.88 wt.%. These textures and the mineral chemistry data indicate refertilization of the previously depleted, MOR-type peridotites by percolating hydrous melts. The whole-rock REE partial melting modeling is consistent with slightly lower degrees of mantle melting (~12–14%) compared to the melt extraction degrees obtained from the Cr-spl compositions (~15%). Chromian spinel (Cr-spl) phases in the cpx-poor harzburgites show a wider variation of Cr#, ranging between 57 and 75, and reflect 30–40% of partial melting. In contrast, the whole-rock geochemistry of these rocks represents slightly lower degrees of partial melting, varying between 30 and 35%. The enrichment of TiO_2 contents of the Cr-spl (up to 0.20 wt.%) in some of the cpx-poor harzburgites can be explained by their interaction with Ti-rich hydrous melt formed at supra-subduction (SSZ) tectonic setting. Highly unradiogenic Os isotope composition (0.11956) of a cpx-poor harzburgite sample suggests an ancient melt depletion event experienced by these rocks, whereas its high Re content is a manifestation of subduction enrichment. The mafic units of the Refahiye ophiolite show MORB-like to island arc tholeiite (IAT) geochemical signatures typical of SSZ oceanic crust. A U–Pb zircon age of 183 ± 1 Ma obtained from an isotropic gabbro sample suggests that the crystallization of the SSZ-type mafic units in the Refahiye ophiolite is as old as the early Jurassic.

1. Introduction

Upper mantle peridotites exposed in ophiolites represent residues after various degrees of melt extraction from the primitive mantle, and hence the fragments of previously depleted, ancient peridotites. For example, lherzolites and cpx-rich harzburgites in ophiolites are commonly regarded as low-degree (5–15%) partial melting residues of the primitive mantle under dry conditions (Dick and Bullen, 1984; Johnson et al., 1990; Niu, 1997, 2004; Hellebrand et al., 2002). In contrast, the in-situ and ancient examples of forearc peridotites are mostly depleted (harzburgites or dunites), and are interpreted to have formed after the extraction of a large proportion of melt (>20%) in hydrous conditions (Ishii et al., 1992; Parkinson et al., 1992; Arai, 1994; Pearce et al., 2000; Uysal et al., 2012, 2013). In both cases, the melting events appear to have resulted in the extraction of melt with various compositions, and to have left behind a depleted mantle residue, whose composition was strongly controlled by the magnitude of melt extraction. The residues after high degrees of melting are commonly highly depleted in incompatible elements, compared to the low-degree melting residues, in both bulk and mineral chemistry.

Recent investigations on some abyssal and ophiolitic peridotites show, however, that there is a major contradiction between the bulk composition and mineral chemistry that cannot be explained with a

* Corresponding author. Tel.: +90 462 3772744; fax: +90 462 3772705.
E-mail addresses: uysal.ibrahim@gmail.com, iuysal@ktu.edu.tr (I. Uysal).

1342-937X/$ – see front matter
http://dx.doi.org/10.1016/j.gr.2013.09.008

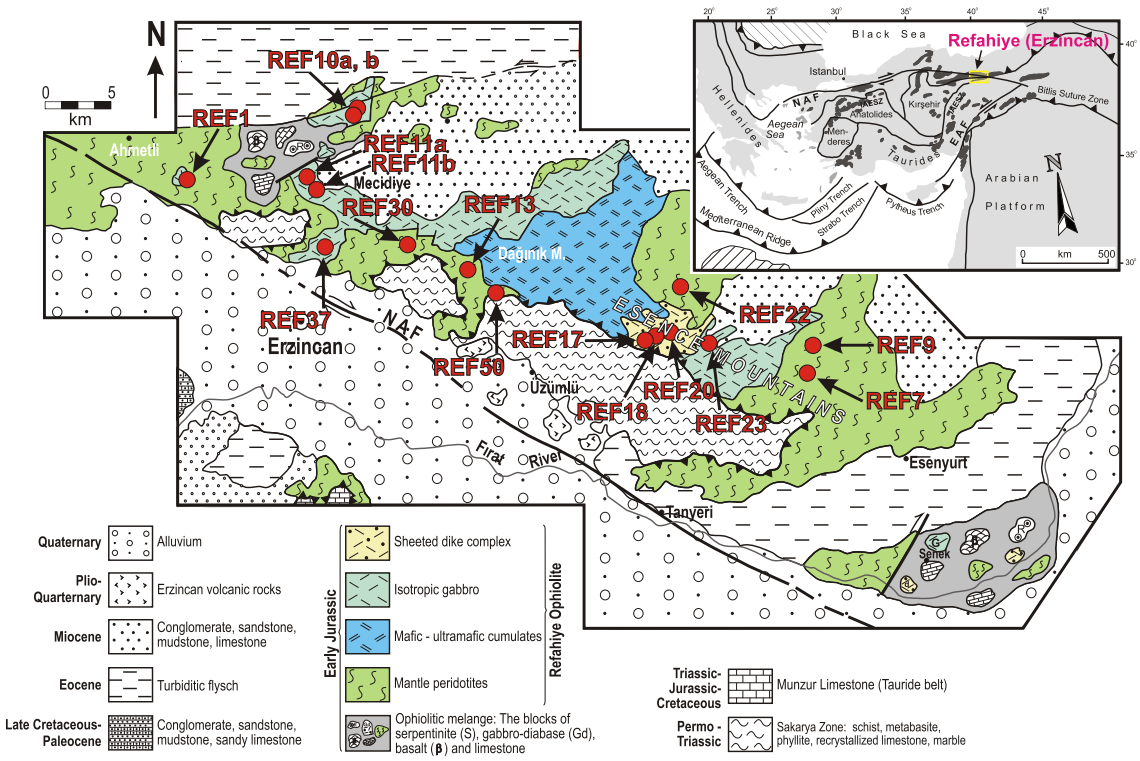

Fig. 1. Simplified geological map of the Refahiye area in NE Anatolia (modified from Aktimur et al., 1995; Özen et al., 2008; Sarifakioglu et al., 2009), showing the peridotite sample locations. Inset map displays the major tectonic belts (Dinter, 1998) and the distribution of major ophiolite complexes in Turkey (Dilek and Furnes, 2009). NAF: North Anatolian Fault, EAF: Eastern Anatolian Fault, IAESZ: Izmir–Ankara–Erzincan Suture Zone.

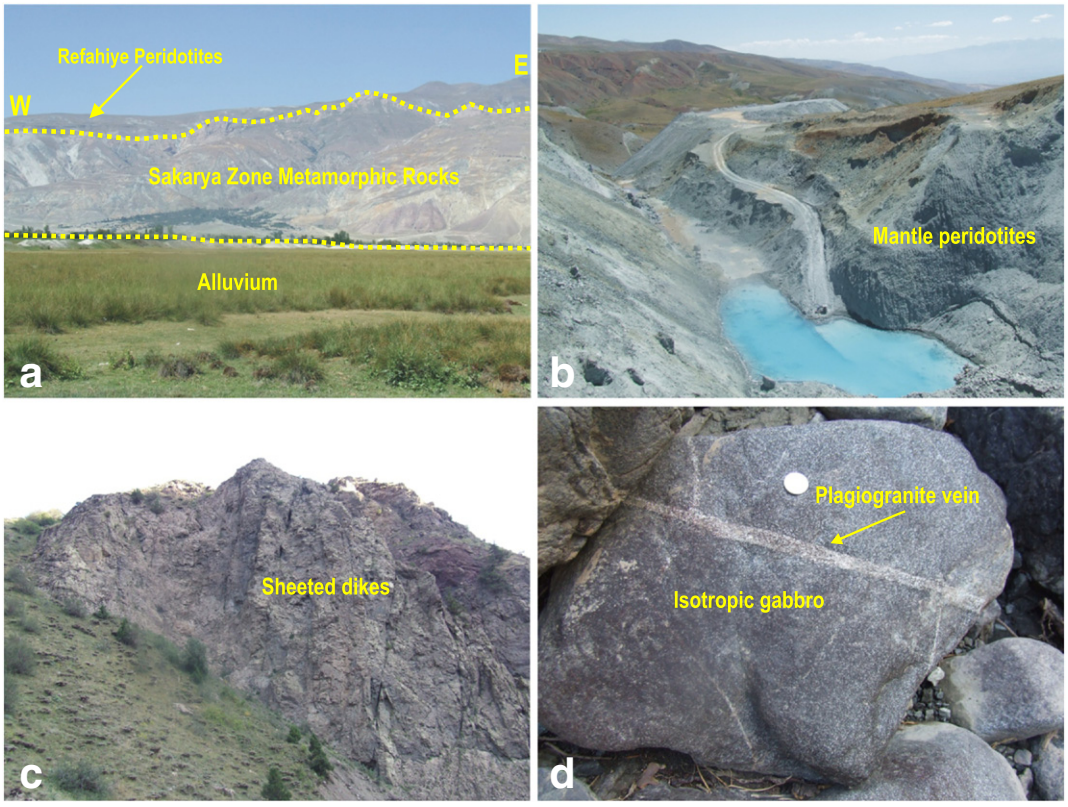

Fig. 2. Field photographs of (a) the upper mantle peridotites tectonically resting on the metamorphic units of the Sakarya Continent, (b) serpentinized upper mantle peridotites in a chromitite mine in the Refahiye ophiolite, (c) doleritic sheeted dike complex in the Refahiye ophiolite, and (d) a plagiogranite vein in an isotropic gabbro in the Refahiye ophiolite.

Table 1
Whole rock major oxides (wt.%), trace elements and REE abundances (ppm) in peridotite samples of Refahiye (Erzincan) ophiolite. LOI: loss on ignition; Mg# = (mol) 100 × MgO / (MgO + FeO); Serp% = (100 / 18) × LOI (wt.%); –: below detection limits; DL: detection limits (wt.% for major oxides and ppm for trace elements and REE); NA: Not analyzed.

	REF13	REF30	REF7	REF9	REF22	REF50	REF1	REF10a	REF10b	RE23
	Cpx-H	Cpx-H	H	H	H	H	IG	IG	IG	IG
Latitude	39.771818	39.768823	39.689833	39.689818	39.823934	39.766413	39.844971	39.892369	39.892369	39.719613
Longitute	39.729033	39.686887	40.170845	40.172279	39.850441	39.728976	39.380409	39.536226	39.536226	39.841049
SiO_2	44.70	44.07	45.91	47.08	41.85	44.38	50.9	42.97	43.87	51.79
TiO_2	0.038	0.049	0.005	0.01	0.003	0.003	0.437	2.357	2.270	0.698
Al_2O_3	2.12	2.05	0.52	0.89	0.16	0.22	17.96	18.29	19.98	18.43
Fe_2O_{3T}	9.04	9.16	9.13	9.20	9.82	9.35	8.13	13.69	12.35	10.44
MgO	41.01	42.18	42.73	40.51	46.46	45.07	7.62	7.48	6.25	5.83
CaO	1.53	1.44	0.19	0.77	0.07	0.11	11.35	12.32	12.50	9.29
Na_2O	0.02	0.02	–	0.01	–	–	3.03	1.97	2.10	2.98
K_2O	–	–	–	0.02	–	–	0.13	0.24	0.25	0.20
P_2O_5	0.02		0.04	0.02	0.04	0.02	–	0.04	0.02	0.05
MnO	0.16	0.12	0.12	0.13	0.08	0.12	0.12	0.19	0.18	0.16
Cr_2O_3	0.42	0.33	0.35	0.45	0.52	0.30	0.02	0.01	0.01	0.01
LOI	13.20	12.36	15.00	13.40	14.90	13.77	3.1	1.90	2.20	2.60
Sum	99.39	99.42	99.39	99.10	99.35	99.58	99.82	99.79	99.77	99.84
Mg#	90.0	90.1	90.3	89.7	90.4	90.5	65.0	52.0	50.1	52.5
Sc	11.6	12.7	8.0		4.9	6.7	31.8	76.9	68.0	40.0
V	50.8	53.5	32.3		4.7	15.3	173	365	346	311
Cr	2517	2017	2086		929	1775	146	27.5	NA	NA
Co	99.5	100.1	107		131	123	30.7	37.0	32.8	36.3
Ni	2219	2175	2514		2851	2907	68.5	9.04	3.3	10.6
Cu	23.85	27.1	13.41		3.728	10.1	8.2	46.23	35.2	4.9
Zn	39.9	39.6	36.1		30.7	40.4	39.9	82.2	25.0	30.0
Ga	1.80	1.65	0.58		0.16	0.29	13.5	17.6	16.2	17.1
Rb	0.129	0.077	0.079		0.086	0.092	0.834	2.94	3.20	1.0
Sr	2.60	1.95	1.96		1.46	1.19	238	271	340	164
Y	1.38	1.80	0.140		0.089	0.070	11.4	31.3	22.5	11.4
Zr	0.506	0.504	0.179		0.071	0.097	13.4	16.8	15.1	12.7
Nb	0.018	0.005	0.005		0.011	0.009	0.544	1.40	1.30	0.7
Cs	0.011	0.011	0.212		0.007	0.027	0.036	0.399	0.300	–
Ba	8.02	0.88	1.51		0.909	2.34	34.1	44.5	43.0	30.0
La	0.0816	0.0100	0.0232		0.0186	0.0167	2.203	1.101	1.100	1.10
Ce	0.1946	0.0846	0.0882		0.0670	0.0861	4.946	3.935	3.700	2.60
Pr	0.0250	0.0094	0.0061		0.0045	0.0038	0.733	0.947	0.740	0.44
Nd	0.1162	0.0966	0.0300		0.0205	0.0266	3.460	6.680	4.800	2.40
Sm	0.0681	0.0790	0.0111		0.0040	0.0058	1.010	3.093	2.220	1.02
Eu	0.0267	0.0318	0.0020		0.0014	0.0031	0.480	1.149	0.960	0.47
Gd	0.1115	0.1420	0.0163		0.0072	0.0064	1.378	4.288	3.430	1.47
Tb	0.0279	0.0349	0.0030		0.0024	0.0020	0.258	0.868	0.670	0.30
Dy	0.1988	0.2523	0.0194		0.0111	0.0083	1.716	5.723	4.220	1.89
Ho	0.0486	0.0624	0.0049		0.0030	0.0022	0.388	1.228	0.830	0.45
Er	0.1509	0.1690	0.0161		0.0109	0.0058	1.111	3.181	2.500	1.30
Tm	0.0244	0.0327	0.0032		0.0016	0.0015	0.182	0.459	0.330	0.21
Yb	0.1690	0.2033	0.0265		0.0146	0.0117	1.221	2.721	1.890	1.28
Lu	0.0281	0.0355	0.0058		0.0031	0.0025	0.200	0.396	0.270	0.19
Hf	0.0274	0.0421	0.0049		0.0023	0.0032	0.544	0.814	0.400	0.50
Ta	0.0016	0.0003	0.0004		0.0006	0.0004	0.037	0.064	–	–
Pb	0.1974	0.2014	0.3056		0.0944	0.3474	0.489	0.971	1.500	0.90
Th	0.0155	0.0017	0.0024		0.0022	0.0039	0.186	0.082	0.100	0.10
U	0.0074	0.0004	0.0009		0.0011	0.0016	0.066	0.049	NA	NA

The average composition calculated from 6 different analyses during the measurements, standard deviation and RSD% values of the internal peridotite standard GP13, as well as the average and standard deviation of blank values of each elements were also included.

simple partial melting event alone (e.g., Roux et al., 2007; Rampone et al., 2008). Crystallization of the interstitial plagioclase and clinopyroxene (cpx) phases from a percolating melt, which results in the refertilization of an already depleted mantle, has been documented as the main cause of change in the composition of the lithospheric mantle in most peridotite massifs (Hebert et al., 1983; Rampone et al., 1997; Dijkstra et al., 2001; Seyler et al., 2001; Borghini et al., 2007; Piccardo et al., 2007; Dilek and Morishita, 2009; Morishita et al., 2011). The upper mantle peridotites in many ophiolites underwent multiple episodes of partial melting, depletion and refertilization events that significantly modified their primary compositions. Documentation of the textural, mineralogical and compositional artifacts of these processes requires, systematic field and integrated petrographic observations, and petrological, geochemical, geochronological and isotope analyses of least altered peridotites.

Suprasubduction zone (SSZ) ophiolites display structural, petrological and geochemical features in their crustal and upper mantle units that commonly indicate the time-progressive development of their ancient oceanic lithosphere in various stages of the Wilson cycle evolution of ocean basins (Dilek and Eddy, 1992; Dilek and Flower, 2003; Flower and Dilek, 2003; Saccani and Photiades, 2004; Barth and Gluhak, 2009; Delavari et al., 2009; Pearce and Robinson, 2010; Dilek and Furnes, 2011; Saccani et al., 2011). For example, the Jurassic–Cretaceous Tethyan ophiolites in the eastern Mediterranean region appear to have evolved during the seafloor spreading and subduction rollback stages of different seaways in the Tethyan realm (Dilek and Flower, 2003; Dilek and Robinson, 2003; Flower and Dilek, 2003; Dilek and Thy, 2009). The ophiolitic fragments within the Izmir–Ankara–Erzincan suture zone (IAESZ) in northern Anatolia are particularly revealing because their crystallization, metasomatism and emplacement ages span a long time window from the early Jurassic (even perhaps earlier) to the late Cretaceous (Sarifakioglu et al., in press), and their upper mantle peridotites constitute the rich archives

REF11b	REF11a	REF37	REF17	REF18	REF20	DL	Blank (average)	GP13 Average	GP13 StDev	GP13 RSD%
IG	IG	IG	SD	SD	SD			Standard	Standard	Standard
39.806674	39.806674	39.799921	39.719491	39.720451	39.732868					
39.520700	39.520700	39.625614	39.840499	39.843626	39.860628					
48.92	53.71	42.53	54.16	52.37	54.38	0.01				
0.613	0.251	0.075	2.045	2.104	1.475	0.001		0.10	0	2.64
16.89	23.81	19.63	14.55	14.36	15.70	0.01				
11.50	4.05	2.81	12.69	14.82	6.94	0.04				
9.47	3.19	7.29	3.65	4.59	4.41	0.01		0.12	0	3.97
8.29	8.39	27.09	6.19	5.28	11.43	0.01				
3.20	5.46	0.23	5.87	5.26	4.92	0.01				
0.36	0.75	0.02	0.21	0.50	0.34	0.01				
0.11	0.08	0.04	0.20	0.21	0.14	0.01				
0.25	0.10	0.12	0.20	0.26	0.11	0.01				
0.10	0.03	0.08	–	–	0.002	0.002				
3.80	4.20	6.30	1.70	2.10	1.70					
99.8	99.95	99.89	99.81	99.78	99.82					
62.0	61.0	83.7	36.3	38.0	55.7					
			34.0	35.0	41.0	0.1300	0.000	15.33	0.84	5.51
			376	375	399	0.0300	0.000	67.41	1.50	2.23
			NA	NA	NA	0.2800	0.000	2193	72	3.13
			31.5	35.0	21.4	0.0700	0.003	90.6	2.16	2.38
			4.8	9.2	3.1	0.3000	0.461	2164	202	9.31
			38.6	47.9	2.4	0.0900	0.000	25.71	0.56	2.18
			24.0	30.0	12.0	0.0290	0.000	33.27	0.84	2.52
			20.7	20.9	13.2	0.0090	0.019	2.24	0.06	2.89
			2.00	7.40	3.20	0.0020	0.000	0.35	0.01	2.07
			84	145	253	0.0050	0.004	10.10	0.16	1.63
			47.3	47.8	25.8	0.0005	0.000	3.55	0.04	1.00
			136.2	138.5	70.6	0.0130	0.012	5.80	0.03	0.47
			3.60	3.7	2.7	0.0033	0.000	0.10	0.00	1.87
			–	2.600	–	0.0024	0.000	0.07	0.00	3.33
			30.0	61.0	44.0	0.0026	0.002	0.58	0.01	2.31
			9.300	7.60	4.300	0.0005	0.0190	0.20	0.00	1.20
			20.500	20.60	11.100	0.0004	0.0020	0.62	0.01	1.01
			3.080	3.15	1.690	0.0001	0.0000	0.12	0.00	0.38
			17.000	15.00	9.200	0.0004	0.0010	0.70	0.01	0.97
			4.750	5.10	2.750	0.0008	0.0000	0.26	0.00	1.17
			1.780	1.58	1.020	0.0001	0.0010	0.10	0.00	1.12
			6.680	6.89	3.810	0.0004	0.0000	0.40	0.01	1.43
			1.250	1.32	0.710	0.0002	0.0000	0.08	0.00	1.12
			7.820	8.07	4.420	0.0004	0.0000	0.54	0.01	1.28
			1.740	1.82	0.970	0.0001	0.0000	0.12	0.00	1.74
			4.980	5.31	2.840	0.0002	0.0000	0.35	0.00	1.24
			0.750	0.77	0.390	0.0001	0.0000	0.06	0.00	1.95
			4.750	4.92	2.650	0.0001	0.0000	0.37	0.01	1.73
			0.740	0.75	0.400	0.0001	0.0000	0.06	0.00	0.71
			4.200	4.00	1.800	0.0003	0.0010	0.18	0.00	1.64
			0.300	0.30	0.200	0.0001	0.0040	0.01	0.00	0.00
			0.700	0.60	0.400	0.0024	0.0000	0.40	0.01	1.98
			0.700	0.80	0.400	0.0001	0.0000	0.01	0.00	5.08
			NA	NA	NA	0.0001	0.0000	0.00	0.00	13.98

of various processes involved in the Tethyan mantle dynamics and evolution.

In this paper, we present a case study from a Tethyan ophiolite in the IAESZ, Refahiye ophiolite (Fig. 1) in NE Anatolia (Turkey), documenting the partial melting, depletion and refertilization history of its upper mantle peridotites in order to better constrain the Tethyan mantle evolution. The new whole-rock major and trace element geochemistry, mineral chemistry, and Re–Os isotope data allow us to distinguish different stages of partial melting and melt–rock reactions experienced by these peridotites, and to put together a coherent explanation for the time-progressive evolution of the Tethyan upper mantle in this region. We also report here new zircon age data from the Refahiye gabbro that provides us with the igneous formation age of the oceanic crust in the Northern Neotethys. Our discussion and numerical modeling on the depletion and refertilization processes experienced by the Refahiye peridotites should have wide applications for the mantle evolution of other ophiolites in different orogenic belts.

2. Geology of the Refahiye ophiolite

The Refahiye ophiolite occurs along the eastern segment of the IAESZ between the Sakarya Continent and the Anatolide–Tauride Platform, and represents a fragment of the Tethyan oceanic lithosphere derived from the Northern Neotethys (Fig. 1; Dilek et al., 1999; Rice et al., 2006). It consists mainly of upper mantle peridotites (Figs. 2a, b), ultramafic–mafic cumulates with wehrlite and layered and isotropic gabbros, and sheeted dolerite dikes (Fig. 2c). Plagiogranite dikes and veins intrude the isotropic gabbro (Fig. 2d) and the sheeted dike complex. The ophiolite is tectonically underlain by a melange, containing blocks of serpentinite, dolerite, pillow basalts with alternating Liassic chert bands and pinkish

limestone, Jurassic limestone with nodular cherts, Jurassic–Cretaceous micritic limestone and pillow basalt with alkaline compositions (Yılmaz, 1985). The presence of the middle–late Triassic seamount fragments in this melange indicates that the Northern Neotethyan seaway was already open at this time (Sarifakioglu et al., in press). This inference is in agreement with our new age data from the gabbroic rocks in the Refahiye ophiolite, as discussed in a later section.

The Refahiye ophiolite is thrust southward over the Munzur Limestone of the Anatolide–Tauride Platform (Fig. 1). The lower Triassic–Campanian Munzur Limestone constitutes the eastern section of the Mesozoic 'Calcareous Axis' of the Tauride Platform (Ricou, 1980; Özgül, 1981), and consists mainly of neritic shelf carbonates. The late Cretaceous–Paleocene turbiditic sedimentary rocks resting unconformably over the ophiolite constrain its emplacement age as the late Cretaceous (Yılmaz, 1985; Yılmaz et al., 1990; Aktimur et al., 1995). Following its emplacement, the Refahiye ophiolite was thrust back onto the Permo-Triassic metamorphic rocks of the Sakarya Continent in the north as a result of continental collision between Eurasia and the Anatolide–Tauride platform (Fig. 1; Okay, 1984; Dilek, 2006). These Permo-Triassic units include variously metamorphosed and deformed volcanic and sedimentary rocks, composed of sericite–calcschist, muscovite–quartz–calcschist, calcschist, quartzite, gneiss and marble (Özgül, 1981) with late Triassic blueschists and eclogite blocks (Okay et al., 2002).

The sedimentary epiclastic rocks overlying the Refahiye ophiolite include basal conglomerates, grading upwards into sandstone, claystone, clayey to sandy limestone. The post-collisional, Lutetian turbiditic flyschoidal and volcanic–sedimentary rocks cover these epiclastic and ophiolitic units, and are in turn unconformably overlain by Miocene terrestrial deposits, including coal and gypsum.

3. Analytical methods

The electron microprobe analyses of olivine (ol), chromian spinel (Cr-spl), orthopyroxene (opx) and clinopyroxene (cpx) were carried out at the Department of Earth and Environmental Sciences in the Ludwig Maximilian University of Munich (Germany) on a Cameca SX-100 system, equipped with a LaB6 cathode. The measurements were done by using the wavelength dispersive spectrometers at 15 kV, 20 nA and 10 to 30 s counting time for silicates (30 s for Al, Ni, Ca; 20 s for Ti, and 10 s for all other elements). For the chromian spinel, counting times of 100 s for Ti, 30 s for Ni, and 10 s for all other elements were employed. A beam diameter of 1 μm was applied. For calibration, natural and synthetic standards were used. Raw data were revised by a PAP (Pouchou and Pichoir, 1984) matrix correction. The amount of Fe^{3+} in the chromian spinel was calculated assuming the ideal spinel stoichiometry, $R^{2+}O\ R^{3+}{}_2O_3$. Mineral chemical data are presented in Supplementary Tables 1 to 5.

Whole-rock samples were analyzed by X-ray fluorescence (XRF) at the ACME Analytical Laboratory at Vancouver (Canada) for major elements. Concentration of the REE (Rare Earth Elements) and some other trace elements (Rb, Sr, Y, Zr, Cs, Ba, Hf, Nb, Ta, U, and Th) were determined by Inductively Coupled Plasma Mass Spectroscopy (ICP-MS) using a Thermo Scientific X-Series2 in the Department of Earth Sciences at the University of Durham, following a standard nitric and hydrofluoric acid digestion (Ottley et al., 2003). The whole analytical procedures are given in Uysal et al. (2012). Detection limits of each element, average blank values as well as average, standard deviations and RSD% values of in-house peridotite standard (GP13) are presented in Table 1.

Selected whole-rock samples of cpx-rich and cpx-poor harzburgites and isotropic gabbros were analyzed for highly siderophile element (HSE: Os, Ir, Ru, Pt, Pd, Re) concentrations and $^{187}Os/^{188}Os$ isotope ratios by the method of isotope dilution, following the technique described by Meisel et al. (2003) and Paliulionyte et al. (2006), on a quadrupole ICP-MS system (HP 7500, Agilent Technologies) at the Montanuniversitaet Leoben, Austria. The results of these analyses are given in Table 2. The whole analytical procedures are as in Uysal et al. (2012).

Zircons from one gabbroic sample (REF1) were separated using standard magnet and heavy liquid separation techniques, and were then handpicked under a binocular microscope. Zircon yield was only 24 grains from 300 g of the rock sample. The separated zircon grains were subhedral with rounded edges and colorless to pale purple, most of which are less than 100 μm along the c-axis. All the zircons were mounted in a PFA Teflon sheet and polished with several diamond pastes. Zircon U-Pb dating for the sample was carried out using an ICP-MS combined with an ArF Excimer laser-ablation sampling technique (e.g., Hirata and Nesbitt, 1995; Iizuka and Hirata, 2004) at the Laboratory for Planetary Science of Kyoto University, Japan. The ICP-MS instrument used in this study was a Nu Instruments (Wrexham, UK) AttoM high resolution-magnetic sector field-ICPMS (Yokoyama et al., 2011). The laser ablation system was a New Wave Research NWR193 laser ablation system (Fremont, CA 94538, USA). In order to determine the ^{238}U-^{206}Pb and ^{235}U-^{207}Pb ages of the smaller grains, an ablation pit sizes of 20 μm and 15 μm were used. Spot-analyses monitoring ^{202}Hg, ^{204}Pb (^{204}Hg), ^{206}Pb,^{207}Pb, ^{232}Th and ^{238}U were performed for core and/or rim of the zircon crystals avoiding inside inclusions, i.e. total 24 spots for 23 grains were measured in this study. The instrumental bias for the $^{206}Pb/^{238}U$ ratio was corrected by normalizing the $^{206}Pb/^{238}U$ ratio to 0.1792 using 91500-Zircon Standard (Wiedenbeck et al., 1995). The OD-3 Zircon (ca. 33 Ma: Iwano et al., 2012) was also used as a secondary standard to check the validity of dating sessions. The results, as well as the instrumentation and operational conditions for U–Pb dating, are listed in Table 3.

4. Petrography

Taking into account the modal abundance of their cpx, the upper mantle peridotites in the Rehafiye ophiolite are divided into two groups: (1) cpx-rich harzburgites (samples REF13 and REF30) and (2) cpx-poor harzburgites (samples REF7, REF9, REF22 and REF50). It is difficult to distinguish these two groups of peridotites in the field. In thin section, the cpx-rich harzburgites show a protoclastic texture as an artifact of intense tectonic deformation and recrystallization (Figs. 3a, b). The rocks contain ol (55–60%), opx (32–34%), cpx (4–5%) and Cr-spl (1–2%), and the interstitial phases of cpx and amphibole (3–4%) (Figs. 3b, c). The cpx-poor harzburgites, on the other hand, have relatively higher ol (75–85%) and Cr-spl (2–3%), and lower opx (8–21%) and cpx (1–2%) contents, and no amphibole, although their textural features are similar to those of the cpx-rich harzburgites (Fig. 3b).

Table 2
Al_2O_3 (wt.%), PGE and Re concentrations (ppb), and Re–Os isotopic data of the selected peridotite and gabbro samples from the Refahiye (Erzincan) ophiolite. Corresponding spinel Cr# values of the peridotite samples are also given in last column. Cpx-rich H: Cpx-rich harzburgite, Cpx-poor H: Cpx-poor harzburgite.

Sample	Rock type	Al_2O_3	Os	Ir	Ru	Pt	Pd	Re	$^{187}Os/^{188}Os$	γOs	Cr# Spl
REF13	Cpx-rich H	2.12	5.01	3.48	7.60	9.15	6.01	0.297	0.12400	−2.36	32.7
REF30	Cpx-rich H	2.05	5.26	4.05	7.31	7.13	5.54	0.343	0.12389	−2.44	34.5
REF50	Cpx-poor H	0.22	5.31	1.71	8.08	2.65	1.10	0.398	0.11956	−5.86	73.5
REF1	Isotropic Gabbro	17.96	0.07	0.11	0.08	0.49	0.20	0.260	0.20738	63	
REF10	Isotropic Gabbro	18.29	0.03	0.06	0.15	0.33	0.58	0.420	0.58422	360	

γOs is calculated using the parameters from Shirey and Walker (1998) and λ for $^{187}Re = 1.666 \times 10^{-11}a^{-1}$ (Smoliar et al., 1996).

Table 3
U–Pb isotopic data for zircon crystals determined by LA-ICP-MS.

Sample name: REF1	Th/U	Isotopic ratios								Age (Ma)						rho
		$^{207}Pb/^{206}Pb$		Error 2σ	$^{206}Pb/^{238}U$		Error 2σ	$^{207}Pb/^{235}U$		Error 2σ	$^{206}Pb/^{238}U$		Error 2σ	$^{207}Pb/^{235}U$		Error 2σ	
Sample REF1																
Laser ablation pit: 20 μm																
REF1 #1R	0.18	0.0480	±	0.0010	0.02831	±	0.000886	0.1855	±	0.0258	180.0	±	5.7	172.8	±	25.9	0.23
REF1 #1C	0.19	0.0558	±	0.0012	0.02856	±	0.000910	0.2173	±	0.0291	181.5	±	5.9	199.7	±	29.1	0.24
REF1 #2C	0.45	0.0511	±	0.0011	0.02964	±	0.000492	0.2067	±	0.0103	188.3	±	3.2	190.8	±	10.4	0.33
REF1 #3C	0.24	0.0477	±	0.0010	0.02879	±	0.000563	0.1873	±	0.0134	183.0	±	3.6	174.3	±	13.5	0.27
REF1 #4C	0.23	0.0479	±	0.0010	0.02903	±	0.000588	0.1896	±	0.0144	184.5	±	3.8	176.3	±	14.6	0.27
REF1 #5C	0.23	0.0521	±	0.0011	0.02923	±	0.000651	0.2078	±	0.0178	185.7	±	4.2	191.7	±	18.0	0.26
REF1 #6C	0.12	0.0498	±	0.0010	0.02922	±	0.000489	0.1984	±	0.0101	185.7	±	3.1	183.8	±	10.2	0.33
REF1 #7C	0.25	0.0492	±	0.0010	0.02868	±	0.000541	0.1926	±	0.0128	182.3	±	3.5	178.8	±	12.9	0.28
REF1 #8C	0.22	0.0513	±	0.0011	0.02892	±	0.000508	0.2023	±	0.0115	183.8	±	3.3	187.1	±	11.6	0.31
REF1 #9C	0.23	0.0508	±	0.0011	0.02759	±	0.000509	0.1912	±	0.0120	175.4	±	3.3	177.7	±	12.1	0.29
REF1 #10C	0.21	0.0494	±	0.0010	0.02885	±	0.000555	0.1946	±	0.0134	183.3	±	3.6	180.5	±	13.5	0.28
REF1 #11C	0.31	0.0504	±	0.0011	0.02763	±	0.000627	0.1901	±	0.0170	175.7	±	4.0	176.7	±	17.1	0.25
REF1 #12C	0.37	0.0490	±	0.0010	0.02896	±	0.000472	0.1935	±	0.0093	184.0	±	3.0	179.6	±	9.4	0.34
REF1 #13C	0.25	0.0506	±	0.0010	0.02955	±	0.000579	0.2038	±	0.0162	187.8	±	3.7	188.3	±	16.3	0.25
REF1 #14C	0.36	0.0512	±	0.0010	0.02840	±	0.000438	0.1981	±	0.0107	180.5	±	2.8	183.5	±	10.8	0.29
REF1 #15C	0.25	0.0482	±	0.0010	0.02961	±	0.000600	0.1943	±	0.0165	188.1	±	3.9	180.3	±	16.6	0.24
REF1 #16C	0.24	0.0495	±	0.0010	0.02726	±	0.000563	0.1839	±	0.0158	173.4	±	3.6	171.4	±	15.9	0.24
Laser ablation pit: 15 μm																	
REF1 #18R	0.28	0.0515	±	0.0013	0.02935	±	0.000606	0.2043	±	0.0182	186.5	±	3.9	188.8	±	18.4	0.23
REF1 #19R	0.36	0.0516	±	0.0013	0.02842	±	0.000399	0.1980	±	0.0104	180.6	±	2.6	183.4	±	10.5	0.27
REF1 #20R	0.23	0.0449	±	0.0012	0.02907	±	0.000828	0.1762	±	0.0241	184.7	±	5.3	164.8	±	24.2	0.21
REF1 #21R	0.31	0.0496	±	0.0013	0.02915	±	0.000562	0.1953	±	0.0163	185.2	±	3.6	181.2	±	16.4	0.23
REF1 #22C	0.34	0.0503	±	0.0013	0.03022	±	0.000598	0.2055	±	0.0176	191.9	±	3.9	189.7	±	17.7	0.23
REF1 #23C	0.34	0.0527	±	0.0014	0.02890	±	0.000659	0.2058	±	0.0204	183.7	±	4.2	190.0	±	20.6	0.23
REF1 #24R	0.22	0.0507	±	0.0013	0.02762	±	0.000715	0.1893	±	0.0220	175.6	±	4.6	176.0	±	22.1	0.22
In-house standard (OD3: 33 Ma)																	
Laser ablation pit: 20 μm																	
OD3 #1	0.51	0.0481	±	0.0010	0.00519	±	0.000118	0.0340	±	0.0032	33.4	±	0.8	34.0	±	3.2	0.24
OD3 #2	0.48	0.0476	±	0.0009	0.00535	±	0.000115	0.0347	±	0.0030	34.4	±	0.7	34.7	±	3.1	0.25
OD3 #3	0.48	0.0474	±	0.0009	0.00522	±	0.000120	0.0337	±	0.0032	33.5	±	0.8	33.7	±	3.3	0.24
Laser ablation pit: 15 μm																	
OD3 #1	0.52	0.0426	±	0.0011	0.00524	±	0.000122	0.0302	±	0.0032	33.7	±	0.8	30.2	±	3.2	0.22
OD3 #2	0.53	0.0494	±	0.0013	0.00510	±	0.000120	0.0341	±	0.0034	32.8	±	0.8	34.0	±	3.5	0.24
OD3 #3	0.56	0.0482	±	0.0012	0.00525	±	0.000125	0.0342	±	0.0035	33.7	±	0.8	34.1	±	3.5	0.23

C, Core; R, Rim.

Olivine grains in the cpx-poor harzburgites are generally coarse, anhedral and locally medium-grained, enclosed by some opx or relict crystals. Orthopyroxene grains are subhedral to anhedral, locally forming clusters of multiple opx crystals (Fig. 3a–c). Large opx grains commonly contain thin exsolution-lamellae of cpx. Cpx grains form medium- to micro-crystals along the intersections of ol and opx, indicating their late-stage origin (Fig. 3a, c). Chromian spinels are generally anhedral, displaying a holly-leaf texture, and forming fine-grained crystals (<0.4 mm) in the cpx-rich harzburgites; the Cr-spl in the cpx-poor harzburgites occur as euhedral to subhedral, and medium-grained crystals (up to 0.6 mm). Subhedral fragments of the interstitial amphibole crystals, up to 0.2 mm in size, are unevenly distributed in the cpx-rich harzburgite samples. Amphibole tends to occur as irregular growth along the rims of opx or cpx crystals, and locally interstitially between the ol grains (Fig. 3c).

Isotropic gabbros contain subhedral to anhedral plagioclase grains (55–65%) with an average grain size of 0.6 mm (Fig. 3e, f), and cpx crystals (45–35%) with grain sizes ranging from 0.2 to 2 mm. Plagioclase is partly replaced by secondary sericite, chlorite and epidote (Fig. 3g, h), whereas cpx is partly to completely transformed into amphibole as a result of uralitization. Sphene and opaque Fe–Ti oxides (Fig. 3h) form the accessory phases in these rocks.

We classify the isotropic gabbros as amphibole-rich (amphibole/plagioclase = 3:1) and amphibole-poor (amphibole/plagioclase = 1.5:1) based on their amphibole contents. The amphibole-rich gabbros exhibit a generally coarse-grained, equigranular texture, and have Fe–Ti oxides up to 2%. Plagioclase in these gabbros is mostly euhedral and only shows minor alteration. However, in the amphibole-poor gabbros with coarse- to fine-grained inequigranular textures the amphibole grains are commonly subhedral to anhedral in shape, and contain partly altered plagioclase crystals. Many amphibole grains in the studied gabbros host relict cpx crystals, indicating that amphibole is pseudomorphed after cpx. Fe–Ti oxides are more abundant in the amphibole-rich gabbros (Fig. 3h) in comparison to the amphibole-poor gabbros, and have anhedral to subhedral crystals varying in size from 0.1 to 0.5 mm.

The dolerite dike rocks display an ophitic texture, containing subhedral plagioclase and secondary anhedral amphibole replacing the cpx. The grain size varies between 0.2 mm and 6 mm (Fig. 3i). The plagioclase grains in the dike rocks are partly to completely transformed to sericite and chlorite as a result of low-grade ocean floor metamorphism. The sphene and opaque Fe–Ti oxides occur as accessory minerals.

5. Geochemical results

5.1. Mineral chemistry

We performed a total of more than 1000 electron microprobe analyses on ol, opx, cpx, amphibole and Cr-spl in the upper mantle peridotites, and amphibole, plagioclase and Fe–Ti oxides in the isotropic gabbro samples from the Refahiye ophiolite. Selected electron microprobe analyses of these different mineral phases in the Refahiye peridotites and isotropic gabbros are presented in Supplementary Tables 1–5. The results of the mineral analyses are summarized in Figs. 4, 5 and 6.

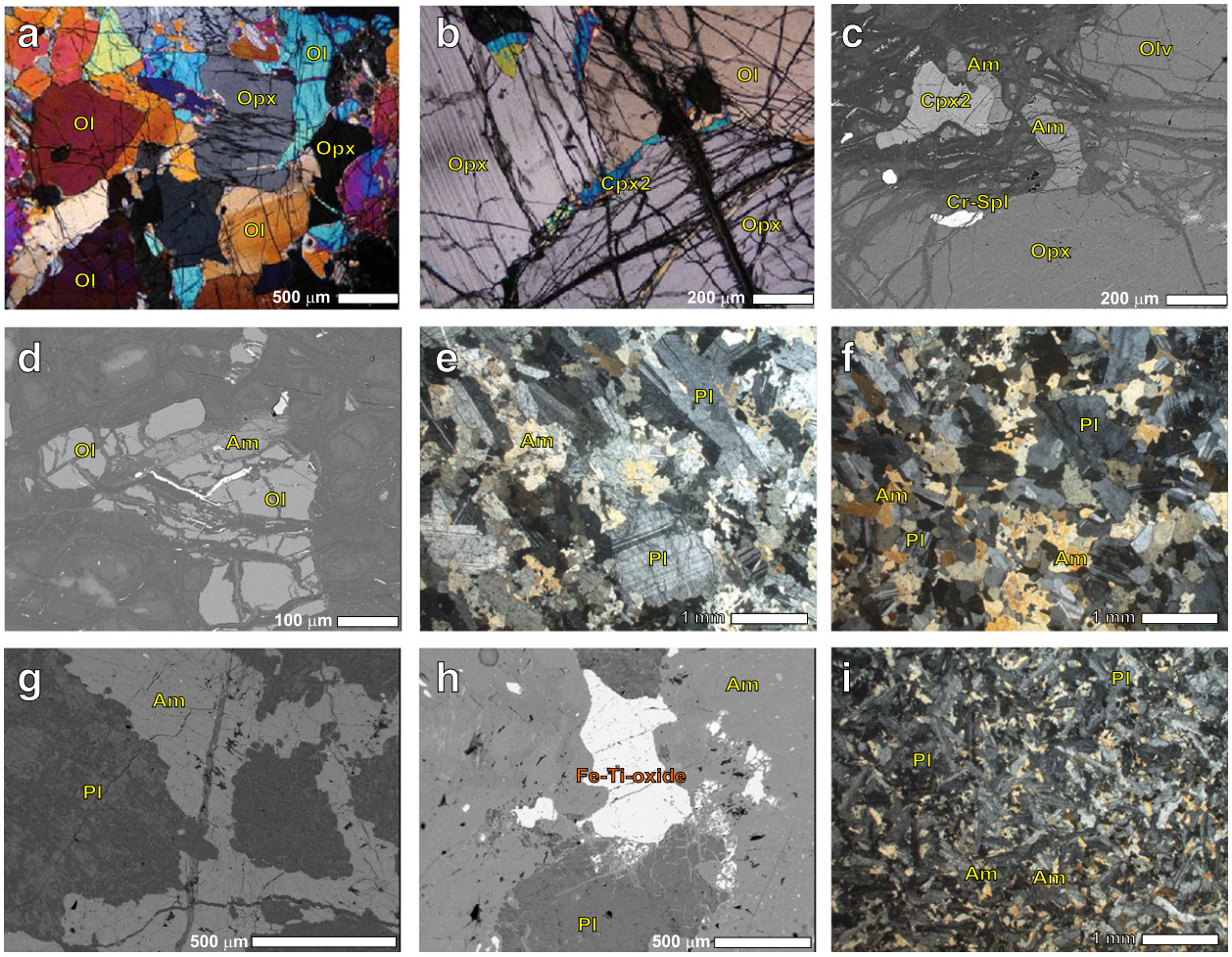

Fig. 3. Plane polarized (crossed-nicol) light (a, b, e, f, i) and back-scattered electron (BSE) images (c, d, g, h) from polished thin sections of the peridotite (a–d), isotropic gabbro (e–h) and sheeted dike (i) samples from the Refahiye ophiolite.

5.1.1. Mantle peridotites

Olivine in the cpx-rich harzburgites is represented by the Fo contents ranging between 89.4 and 90.1, and the NiO content of 0.28–0.44 wt.% (Fig. 4a). However, the Fo contents of ol in the cpx-poor harzburgites are slightly higher (89.4–93.6) than those in the cpx-rich harzburgites, and their NiO contents range between 0.24 and 0.56 wt.%. The MnO contents of ol in both rock types are between 0.06 and 0.17 wt.%, and the CaO content is very low, less than 0.09 wt.% for all samples (Supplementary Table 1).

The Mg# [$100 \times Mg/(Mg + Fe^{2+})$] of opx in the cpx-poor harzburgites range between 90.0 and 92.5, whereas these values show a highly narrow variation ranging from 89.7 to 90.9 in the cpx-rich harzburgites. The cpx-rich harzburgites contain opx with higher Al_2O_3 (1.23–3.02 wt.%) and Cr_2O_3 contents (0.16–1.34 wt.%) than those in the cpx-poor harzburgites, in which the Al_2O_3 and Cr_2O_3 contents vary between 0.22 and 1.64 wt.%, and 0.05 and 0.60 wt.%, respectively. The CaO content of opx in both rock types reaches up to 1.92 wt.% (Supplementary Table 2).

The Mg# values of cpx in the cpx-rich harzburgites range between 91.3 and 93.9, and are lower than those in the cpx-poor harzburgites (93.5–95.5). In contrast, the Al_2O_3 content of cpx in the cpx-rich harzburgites is higher (2.17–3.07 wt.%) than those in the cpx-poor harzburgites (0.83–1.95 wt.%). Similarly, the TiO_2 and Na_2O contents of cpx are more enriched in the cpx-rich harzburgites, ranging between 0.18 and 0.41 wt.%, and 0.12 and 0.25 wt.%, respectively (Fig. 4b). These values are lower in the cpx-poor harzburgites; the TiO_2 and Na_2O contents are less than 0.16 wt.% and 0.17 wt.%, respectively. Chromium behaves in the same manner; its content is higher in the cpx-rich harzburgites (0.53–1.04 wt.% Cr_2O_3) than those in the cpx-poor harzburgites (0.32–0.85 wt.% Cr_2O_3) (Supplementary Table 3).

Chromian spinel phases in the cpx-rich harzburgites are classified as *spinel*, whereas those in the cpx-poor harzburgites are classified as *chromite* to *Mg-chromite*, on the basis of their Cr# and Mg# values (not shown). However, to avoid any misunderstanding, we use in this study the term *chromian spinel (Cr-spl)* for all these phases in different rock types. The cpx-rich harzburgites are represented by Cr-spl of lower Cr# (32–38) and higher Mg# (61–68), whereas the cpx-poor harzburgites contain Cr-spl with higher Cr# (57–75) and lower Mg# (40–55) (Fig. 5). The Cr-spl compositions in the cpx-rich harzburgites plot within the abyssal peridotites field, whereas those of the cpx-poor harzburgites plot within the forearc peridotite field (Fig. 5). The TiO_2 content of Cr-spl is low in the cpx-rich harzburgites, but some samples contain Cr-spl with higher TiO_2 contents up to 0.24 wt.%. The cpx-poor harzburgite samples contain Cr-spl with higher Cr# and lower TiO_2 contents (<0.10 wt.%). However, some of the cpx-poor harzburgite samples contain Cr-spl with higher TiO_2 contents (up to 0.22 wt.%) that is inconsistent with their high Cr# (>60) values. The Fe_2O_3 contents of Cr-spl in the cpx-poor harzburgites are higher (1.63–6.00 wt.%) than those in the cpx-rich harzburgites (1.30–2.13 wt.%) (Supplementary Table 4).

Amphiboles in the cpx-rich harzburgites (samples REF13 and REF30) are pargasitic to edenitic in composition (Fig. 6a), belonging

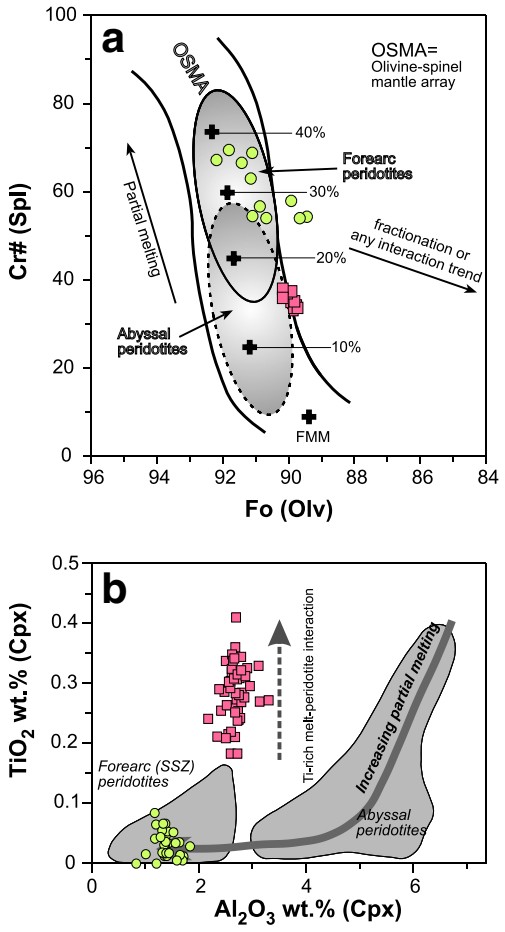

Fig. 4. (a) Compositional relationship between Cr# of the Cr-spl and the Fo [100 × Mg/(Mg + Fe^{2+})] content of coexisting ol (Arai, 1992) in the Refahiye peridotite samples. FMM: Fertile MOR Mantle. (b) TiO_2 (wt.%) versus Al_2O_3 (wt.%) contents in cpx of the peridotite samples. Fields for abyssal and forearc peridotites are taken from Hebert et al. (1990), Johnson et al. (1990), Ishii et al. (1992). Pink squares represent the cpx-rich harzburgites whereas green circles represent the cpx-poor harzburgites.

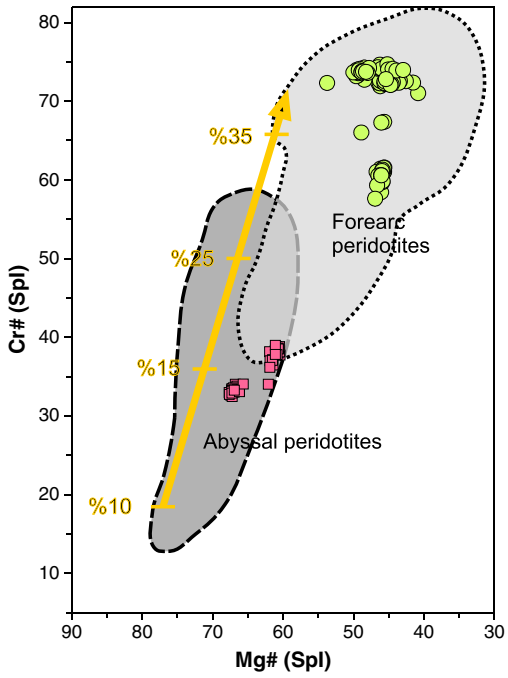

Fig. 5. Compositional relationship between Cr# and Mg# of the Cr-spl in the peridotite samples. Abyssal peridotite field is from Dick and Bullen (1984) and Arai (1994), forearc peridotite field is from Ishii et al. (1992) and Parkinson and Pearce (1998). Partial melting trend is from Arai (1992).

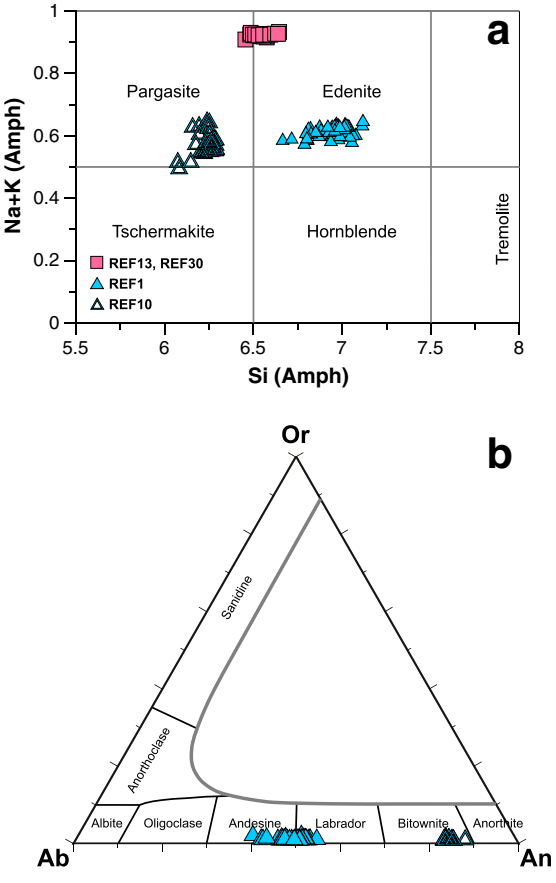

Fig. 6. Classification diagrams of the amphibole (a) and plagioclase (b) grains in the peridotite and gabbroic samples from the Refahiye ophiolite.

to the calcic amphibole group (Leake et al., 1997). They are highly magnesian with Mg# of 91–93, and have variable contents of both Al_2O_3 (8.90–13.31 wt.%) and Cr_2O_3 (1.27–1.93 wt.%). Furthermore, they contain low abundances of Na_2O (1.17–2.16 wt.%) and TiO_2 (0.69–0.88 wt.%) (Supplementary Table 5).

5.1.2. Isotropic gabbros

Amphibole in the amphibole-rich gabbro (sample REF10) is pargasitic in composition, and are characterized by a wide range of Mg# (42–65), Si contents between 6.1 and 6.3 (p.f.u.), and a narrow range of Na + K (0.50–0.65 p.f.u.) contents. However, the amphibole in the amphibole-poor gabbro (sample REF1) is edenitic in composition (Fig. 6a) with a Mg# ranging between 56 and 64, higher Si (6.6–7.2 p.f.u.), and has almost similar Na + K contents (0.57–0.63 p.f.u.) (Supplementary Table 5). Plagioclase in the amphibole-rich gabbro is more calcic ($An_{84–89}$) and Fe rich (up to 0.56 wt.%) than those in the amphibole-poor gabbros ($An_{40–54}$; up to 0.22 wt.% FeO) (Fig. 6b). Plagioclase in both types of the gabbros is represented by a very low content of K_2O (<0.21 wt.%) (Supplementary Table 5). Fe–Ti oxide grains have the TiO_2 contents ranging between 47.56 and 53.36 wt.% and MnO contents between 1.62 and 3.27 wt.% (Supplementary Table 5). The MgO contents of Fe–Ti oxides are low (0.05–0.28 wt.%), suggesting their crystallization at a late stage.

5.2. Whole-rock major and trace element geochemistry

5.2.1. Upper mantle peridotites

The Al_2O_3 and CaO contents of the cpx-rich harzburgites range between 2.05–2.12 wt.% and 1.44–1.53 wt.%, respectively, and are represented by Mg# of 89.2–90.1. However, the cpx-poor harzburgite samples contain a lower content of Al_2O_3 (0.16–0.89 wt.%) and CaO (0.07–0.77 wt.%) and their Mg# vary from 89.7 to 90.5.

The main differences in the mineral chemistry are also displayed by the whole-rock rare earth element (REE) abundances of the peridotites. On a primitive mantle (PM)-normalized REE diagram (Fig. 7), both types of peridotites show similar REE abundances increasing from medium to heavy REE; however, the cpx-rich harzburgites are characterized by higher abundances of medium and heavy REE with respect to those of the cpx-poor harzburgite samples (Table 1). The enrichment of peridotites in light REE commonly produces U-shaped REE patterns, and is commonly reminiscent of forearc to backarc peridotites. This enrichment signature is more developed in the cpx-poor harzburgites in comparison to the cpx-rich harzburgites in the Refahiye ophiolite.

5.2.2. Isotropic gabbros and sheeted dikes

Major and trace element concentrations of the analyzed isotropic gabbro and sheeted dike samples are presented in Table 1. The SiO_2 and TiO_2 contents of the isotropic gabbro samples range between 42.97 wt.% and 53.71 wt.% (mean 47.81 wt.% SiO_2) and 0.07 wt.% and 2.55 wt.% (mean 0.99 wt.% TiO_2), respectively. The sheeted dike samples are represented by higher SiO_2 (52.37–54.38 wt.%; mean 53.64 wt.%) and TiO_2 (1.48–2.10 wt.%; mean 1.87 wt.%) contents in comparison to the isotropic gabbros. However, the CaO (5.28–11.43 wt.%; mean 7.63 wt.%) and MgO (3.65–4.59 wt.%; mean 4.21 wt.%) contents are lower in the sheeted dike samples than those in the isotropic gabbros (8.29–27.09 wt.%, mean 12.75 wt.% CaO and 3.19–9.47 wt.%; mean 6.73 wt.% MgO). Although the Mg# values of the isotropic gabbro samples generally range between 65.0 and 50.1, one sample (REF37) has a higher Mg# value of 83.7. The samples from the sheeted dike complex have lower Mg# values, ranging from 55.7 to 36.3, in comparison to the isotropic gabbros.

An isotropic gabbro sample (REF10A) displays N-MORB (Normal Mid-Ocean Ridge Basalt)-like REE patterns with slight enrichment of middle REE (up to 9 × PM) and depletion of light REE (down to 2 × PM), compared to the heavy REE (6 × PM) contents on a PM-normalized REE plot (Fig. 7). However, sample REF10B has comparable but lower REE contents than those of sample REF10A, and shows slightly depleted heavy REE (4 × PM) and light REE (2 × PM) patterns with almost similar middle REE (6 × PM) contents compared to the N-MORB. Samples REF1 and REF23, both depleted in heavy REE contents compared to N-MORB, show almost flat PM-normalized heavy to middle REE patterns (3 × PM) with very weak Eu positive anomalies. However, compared to sample REF23, sample REF1 shows stronger light REE enrichment, resulting in almost flat REE patterns from Lu to La. In contrast, sample REF23 shows depletion from Sm (2.37 × PM) to Ce (1.46 × PM) and a very slight positive slope from Ce to La (1.60 × PM), representing a spoon-shaped REE pattern. Samples from the sheeted dike complex have almost flat REE patterns below and slightly above the 10 × PM line.

5.3. Whole-rock highly siderophile elements (HSE) and Re–Os Isotope systematics

Highly siderophile elements (HSE) plus Re concentrations and Os isotopic compositions of the peridotite and isotropic gabbro samples are listed in Table 2. The total HSE contents of the upper mantle peridotites (18.9–31.2 ppb), although low, are significantly higher than those presented by the isotropic gabbros (0.95–1.14 ppb). On a PM-normalized diagram (Fig. 8), the cpx-rich harzburgite samples are characterized by almost flat patterns from Os to Re. However, the cpx-poor harzburgites, although their Os, Ru, and Re contents are similar to those of the cpx-rich harzburgites, have lower Ir, Pt, and Pd contents than those of the cpx-rich harzburgites and the primitive mantle values. Two gabbro samples have very low and comparable mantle normalized HSE patterns characterized by a positive slope from Os to Re, consistent with the compatible behavior of Os and the mildly incompatible behavior of Re (Fig. 8).

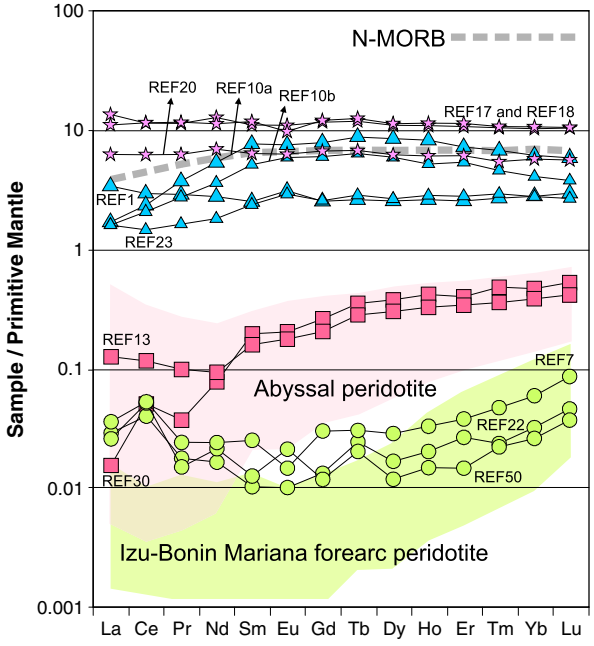

Fig. 7. Primitive mantle-normalized (Palme and O'Neill, 2004) REE diagram for the Refahiye ophiolite samples.
Fields for abyssal and Izu–Bonin Mariana forearc peridotites are taken from Parkinson and Pearce (1998).

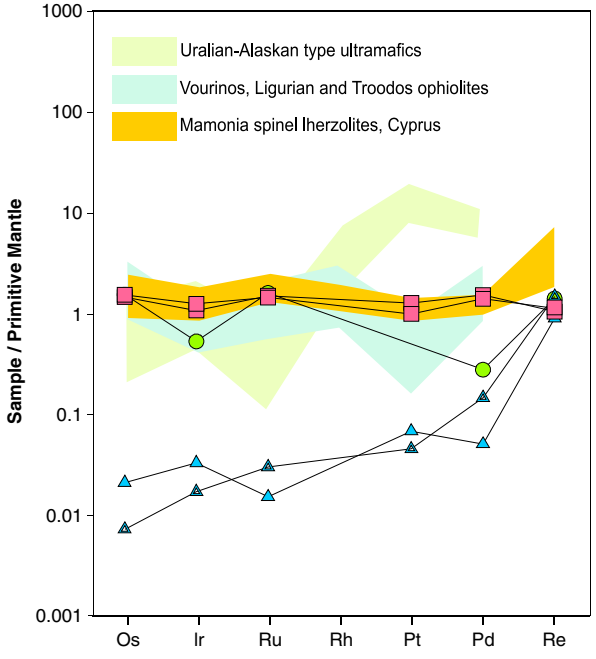

Fig. 8. Primitive Mantle-normalized (McDonough and Sun, 1995) HSE diagram for the Refahiye ophiolite.
Fields for the Uralian–Alaskan type ultramafic rocks, the Vourinos (Greece), Ligurian (Italy) and Troodos (Cyprus) ophiolites, and the Mamonia spinel lherzolites (Cyprus) are taken from Garuti et al. (1997) and Batanova et al. (2008).

The rhenium concentrations of the three peridotite samples range from 0.297 to 0.398 ppb, all higher than the primitive mantle (PM) value of 0.28 ppb (McDonough and Sun, 1995). Their Os contents are also much higher than the PM values and vary between 5.01 and 5.31 ppb. In contrast, the gabbro samples contain much lower Os (0.03–0.07 ppb) but similar Re concentrations (0.255–0.419 ppb) compared to those of the peridotite samples. The amphibole-poor gabbro (REF1) with more sodic plagioclase has 0.255 ppb Re, which is slightly lower than the PM value, and 0.07 ppb Os. However, the amphibole-rich sample (REF10) has higher Re (0.419 ppb) and lower Os (0.03 ppb) contents.

The $^{187}Os/^{188}Os$ isotope ratios of the peridotite samples range between 0.11956 and 0.12400, lower than the estimated Os isotopic ratio of the primitive upper mantle (0.1296; Meisel et al., 2001). The cpx-poor harzburgite samples have the least radiogenic Os isotopic value (0.11956). The isotropic gabbro samples have higher Re/Os ratios that allow the production of more radiogenic $^{187}Os/^{188}Os$ ratios in time, compared to their parental mantle source, which has a much lower Re/Os ratio. The gabbro sample with higher Os content (0.07 ppb) produced less radiogenic $^{187}Os/^{188}Os$ of 0.2074, whereas the Os-poor gabbro sample (0.03 ppb) evolved to an Os isotopic composition of 0.5842 (Table 2).

6. Zircon U–Pb ages

We present twenty-four zircon U–Th–Pb analytical data in Table 3. Uncertainties of isotopic ratios and U–Pb ages are 2σ. The results show concordant data between the $^{206}Pb/^{238}U$ and $^{207}Pb/^{235}U$ ratios (Fig. 9), and the ^{238}U–^{206}Pb ages cluster around 185 Ma (Fig. 9) regardless of the analyzed spot-position (core or rim). There is no common-Pb contamination, Pb-loss, or occurrence of older detrital grains. Therefore, we have obtained a weighted ^{238}U–^{206}Pb age of 183.0 ± 0.7 Ma (n = 24) as a single age population. The analysis of OD-3 zircon yielded a weighted mean ^{238}U–^{206}Pb age of 33.61 ± 0.32 Ma (2σ, n = 6), indicating accurate U–Pb analyses during the session.

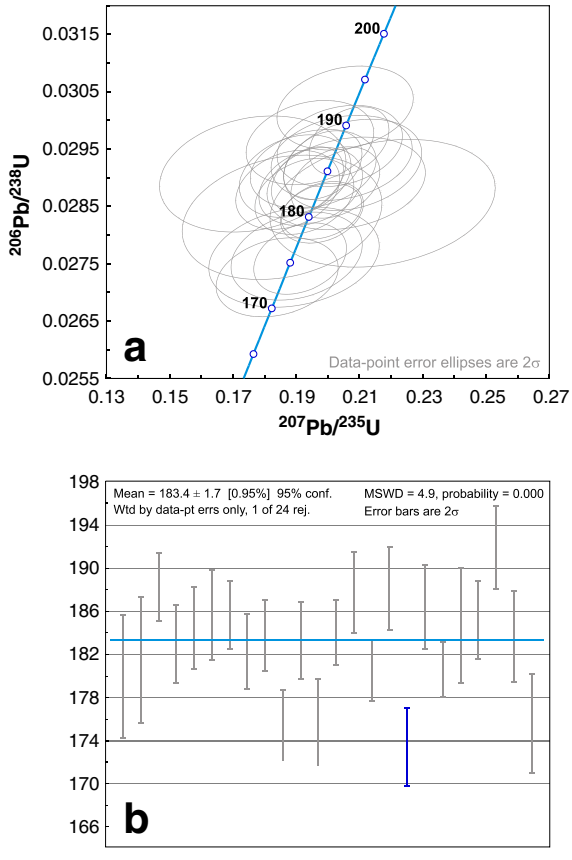

Fig. 9. U–Pb concordia diagram of zircons from the isotropic gabbro sample (REF1) in the Refahiye ophiolite.

7. Discussion

7.1. Origin of the Cpx-rich and Cpx-poor harzburgites

The cpx modal abundances as well as the major and trace element contents of mantle peridotites provide useful information on the melt extraction conditions experienced during the mantle evolution. The very low cpx modal abundance, higher Mg# of the whole-rock samples, and low Al_2O_3 and heavy REE abundances of the cpx-poor harzburgites in the Refahiye ophiolite imply that they experienced higher extents of melt extraction than those of the cpx-rich harzburgite samples. We infer that the rapid depletion of the middle REE compared to the heavy REE of the cpx-poor harzburgites resulted from higher degrees of melting. The depleted- to highly-depleted nature of heavy and middle REE of the harzburgite samples (REF7, REF22, REF50) on the PM-normalized diagram (Fig. 7) confirms that these samples are the residues of higher degrees of melting than those of the cpx-rich harzburgite samples. The heavy to middle REE compositions of these samples resemble those of the Izu–Bonin Mariana forearc peridotites, although the middle and light REEs in the Refahiye peridotites are more enriched compared to those of the Izu–Bonin Mariana peridotites. These features may suggest the addition of higher amounts of slab-derived fluids to the mantle wedge of the Refahiye ophiolite. Slab-derived fluids are known to enrich the overlying mantle, especially in fluid mobile elements (e.g., Ba, Cs, Rb) and LREE (Saunders et al., 1991; Elliott et al., 1997). However, slight enrichment of MREE compared to those of the Izu–Bonin Mariana forearc peridotites may also require some extent of melt addition to the overlying mantle. In contrast, the higher content of Al_2O_3 and lower Mg#, as well as the higher heavy and middle REE contents of the cpx-rich harzburgite samples, suggest that they are the residue of lower-degrees of partial melting. Their PM-normalized REE patterns plot within the abyssal peridotite field and show slight depletion of the MREE compared to the HREE, indicating low-amount of melt extraction during the partial melting processes (Fig. 7). Consequently, we interpret the Refahiye ophiolite peridotites as the low- and high-degree residues of different partial melting events. The low-degree depletion in the cpx-rich harzburgites can be attributed to a first-stage partial melting event that occurred in a mid-ocean ridge (MOR) environment. On the other hand, the high-degree depletion, accompanied by more enrichment in light REE abundances of the cpx-poor harzburgites can be considered as a result of a second-stage partial melting event that took place in a suprasubduction zone (SSZ) environment.

The Cr-spl, which is regarded as a useful phase for the estimation of partial melting processes in mantle peridotites (Arai, 1994; Bédard et al., 2009), also show two distinct compositions between the two types of peridotites in Refahiye. The Cr-spl from the cpx-rich harzburgites is r-epresented by higher Mg# and lower Cr#, suggesting 14–18% partial melting. The cpx-poor harzburgites contain Cr-spl with lower Mg# and higher Cr#, suggesting 30–40% partial melting (Fig. 4a). These partial melting degrees are generally in agreement with the PM-normalized heavy REE contents of the samples (Fig. 7). The diagram of Cr# of the Cr-spl versus the Fo content of ol (OSMA: Olivine Spinel Mantle Array; Arai, 1994) shows that the two groups of the analyzed samples plot within two different fields (Fig. 4a). The cpx-poor harzburgites plot mainly within the field for forearc peridotites, whereas the cpx-rich harzburgites fall within the field of abyssal peridotites. Therefore, we suggest that the cpx-rich harzburgites represent the residue after low-degrees of melting during the first stage partial melting event at a mid-ocean ridge (MOR) tectonic setting. The cpx-poor harzburgites, on the other hand, represent the residues of higher degrees of melting of the previously depleted peridotites (cpx-rich harzburgites) that likely occurred in a SSZ tectonic environment.

7.2. Geochemistry and tectonic setting of isotropic gabbros and sheeted dikes

The isotropic gabbro samples REF10A and REF10B show N-MORB, and sample REF1 displays enriched mid-ocean ridge basalt (E-MORB)-like geochemical signatures based on their REE patterns. However, sample REF23 exhibits a concave-upward REE pattern, typical of boninites (Dilek and Furnes, 2011). The REE patterns of the doleritic sheeted dike samples suggest that they formed from fractionated island-arc tholeiite (IAT)-type melts.

The isotropic gabbro samples of REF10B and REF23 are characterized by lower Nb/Yb (0.55–0.69) ratios that are typical for N-MORB to depleted MORB. However, samples REF10A and REF1 have higher Nb/Yb ratios of 1.14 and 1.40, respectively, showing geochemical similarities to the E-MORB. Samples REF1, REF10A and REF10B, with their lower Th/Yb ratios, plot within the MORB-OIB (ocean island basalt) array, whereas sample REF23 shows subduction influence with its lower Nb/Yb and slightly higher Th/Yb ratio (0.08). However, samples REF17, REF18 and REF20 from the sheeted dike complex have similar Nb/Yb ratios with those of the isotropic gabbro samples, but display higher Th/Yb ratios (~0.16) indicating subduction-related enrichment of their melt source (Fig. 10a).

These samples were evaluated also on a V versus Ti diagram (Fig. 10b). The isotropic gabbro samples REF1 and REF23 plot within the IAT field with their lower Ti and V contents, whereas samples REF10A and REF10B have higher Ti contents due to a higher modal abundance of Fe–Ti oxides, and hence plot within the overlapping MORB-BABB (Back-arc basin basalt) fields. However, nearly all the analyzed samples from the sheeted dike complex plot within the MORB-BABB field. The higher Th/Yb ratios of all the sheeted dike samples suggest that their origin was more likely to be affiliated with a subduction setting than a MOR setting. Although the isotropic gabbro samples REF1 and REF23 plot within the IAT field on a V versus Ti diagram, one of these two samples, REF1, remains within the MORB-OIB array on the Th/Yb versus Nb/Yb diagram showing no subduction influence. In the same way, sample REF10A plots within a MORB-BABB field on the V versus Ti diagram and in the MORB-OIB array on the Th/Yb versus Nb/Yb diagram. These two samples (REF1 and REF10A) probably formed from melts which evolved in a trench-distal BAB tectonic environment (Dilek and Furnes, 2011; Furnes et al., 2012), where lesser amounts of subduction-derived fluids were incorporated into the melt column beneath the BAB spreading center, compared to the arc or forearc tectonic environments (Reagan et al., 2010; Dilek and Furnes, 2011; Ishizuka et al., 2011).

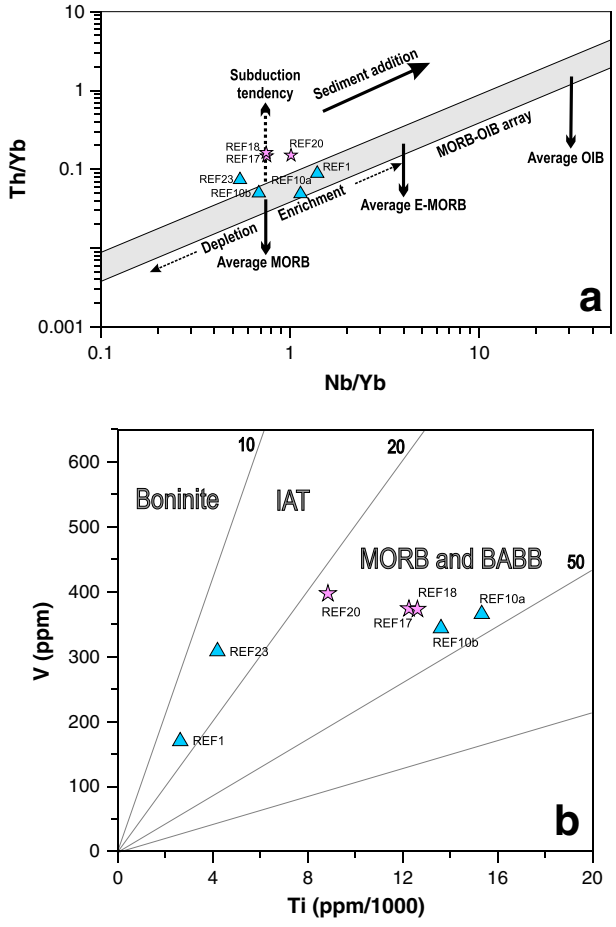

Fig. 10. Th/Yb versus Nb/Yb (a; Pearce, 2008) and V versus Ti (b; Shervais, 1982) plots for the isotropic gabbro and sheeted dike samples from the Refahiye ophiolite.

7.3. Formation of amphibole in cpx-rich peridotites

Pargasitic to edenitic amphiboles commonly occur interstitial to ol or on the rims of fresh opx and cpx crystals in the cpx-rich harzburgites (Fig. 3c). These amphiboles likely formed as a result of the reaction of fluids or melts with cpx and opx grains; thus, the amphibole compositions can help us identify the nature of melts or fluids as metasomatizing agents introduced into the mantle peridotites. Amphiboles in mantle xenoliths from subduction zone settings generally have low Ti contents compared to those from intraplate settings (Coltorti et al. (2007). Hence, the low Ti content of amphiboles (0.69–0.88 wt.% TiO_2) in the cpx-rich harzburgites of the Refahiye ophiolite may indicate their origin from subduction-derived fluids/melts. Overall, the amphibole compositions in the cpx-rich peridotites are similar to those amphiboles documented from mantle wedge peridotites (Ishimaru et al., 2007; Arai and Ishimaru, 2008) and to those reported from the Yungbwa peridotites in southern Tibet (Liu et al., 2010). Therefore, we infer that the amphiboles in the cpx-rich harzburgites formed as a result of the percolation and reaction of slab-derived hydrous fluids/melts through and with the peridotites, which were the mantle residues following an earlier partial melting experience at a MOR setting. The interstitial cpx in these harzburgites is also a product of melt interaction with the slightly depleted mantle (e.g., Hellebrand et al., 2002; Roux et al., 2007; Seyler et al., 2007). Amphiboles may precipitate due to the reaction of metasomatic agents with the pre-existing cpx or directly from the percolating melts. Our petrographic observations suggest that the amphiboles in the cpx-rich harzburgites formed directly from the percolating melts.

7.4. Implications on metasomatism and refertilization

7.4.1. Petrographic and major-trace element evidence

The interstitial texture of ol, cpx and amphibole in the cpx-rich harzburgites suggests that these phases were crystallized from low-volumes of hydrous melt percolated through the upper mantle peridotites. Low-degrees of partial melting produce low-quantities of melt, enriched mainly in light REE. As this melt percolates through and gets trapped in the upper mantle peridotites, hydrous mineral phases precipitate interstitially (Fabriès et al., 1989). Since both the cpx and amphibole are the main carriers of middle and heavy REE, it would be expected that melt percolation would re-equilibrate (or increase) the REE abundances of the upper mantle peridotites (Witt-Eickschen and Harte, 1994; Gaetani, 2004). Such metasomatism would cause the addition of middle and heavy REE to the mantle peridotites, a process known as refertilization, which produces geochemical features similar to their less depleted equivalents (e.g., Ulrich et al., 2010). Therefore, the present REE budget of the cpx-rich harzburgites in Refahiye, shown in Fig. 7, does not reflect the original REE budget of the first-stage, low-degree partial melting residue (MOR-type peridotites). The addition of REE via the interstitial phases of cpx and amphibole that were trapped during the

melt percolation increased the REE abundances in the final composition of the cpx-rich harzburgites.

We compared the mineral compositions of the cpx-rich Refahiye harzburgites to those of the cpx-rich harzburgites of the Cretaceous Muğla ophiolite in SW Turkey. The cpx-rich Muğla harzburgites are interpreted to have formed mainly by dry melting in a MOR setting (Uysal et al., 2007, 2012). The Cr-spl Cr# of the Muğla peridotites is ~15–21, and their middle to heavy REE abundances (e.g., Yb_N = 0.25–0.41) are modeled to have resulted from 10 to 16% melting of a primitive mantle source. The Cr# values of the Cr-spl from the interstitial ol-, cpx- and amphibole-bearing cpx-rich harzburgites of the Refahiye ophiolite are considerably higher than those of the Muğla samples (between 32 and 38). However, the middle to heavy REE abundances of the Refahiye samples (e.g., Yb_N = 0.37–0.44) are still comparable to those of the Muğla samples. We, hence, infer that the Refahiye samples should have formed via higher degrees of melting with respect to the Muğla samples, but that their REE budgets should have also been increased by melt addition, as indicated by the presence of secondary amphibole and cpx as a carrier of the medium to heavy REE. The slight enrichment of the light REE in the cpx-rich Refahiye harzburgites may also be explained by the interaction of hydrous melts with the overlying mantle peridotites that might have developed synchronously with the formation of secondary amphibole and cpx.

The U-shaped REE patterns are commonly seen in highly depleted peridotites (Dilek and Thy, 2009; Dilek and Furnes, 2011). The enrichment of the light REE against depletion of the middle REE is commonly attributed to the interaction of depleted peridotites with melts or fluids enriched in light REE. Although most of the ol from the highly depleted Refahiye peridotites plot within OSMA, confirming their mantle residue origin, some ol in both sets of the sample suites (cpx-rich and cpx-poor) plot outside of OSMA. This type of ol with a lower Fo content precipitates from the fractionated melt, which forms the cumulate section of ophiolites, or can crystallize from a more fertile melt. Our petrographic observations of the both types of peridotite samples show no cumulate texture, and hence we consider these ultramafic rocks as mantle peridotites. Therefore, we suggest that the compositional trend of ol in Fig. 4a was a result of melt–peridotite interaction, rather than fractionation.

The Cr-spl compositions also show the evidence of interaction of melts with different compositions. The lower-degree partial melting residue of the cpx-rich harzburgites is represented by a lower Cr# of the Cr-spl (32–38), and the TiO_2 content of these Cr-spl shows a wide variation (0.13–0.24 wt.%) (Fig. 11). Titanium is incompatible during partial melting and its content is expected to decrease as the melting degree increases (Kinzler and Grove, 1992; Langmuir et al., 1992; Pearce et al., 2000; Choi et al., 2008). However, such high content of Ti in the Cr-spl grains in the cpx-rich harzburgites cannot be interpreted by partial melting alone, and requires further explanation for this increase. Pearce et al. (2000) have suggested that the interaction of MORB-type melts may increase the Ti content of Cr-spl in depleted mantle peridotites, without changing the Cr content. MORB-type melt can be produced in both MOR and back-arc spreading settings. Therefore, the interaction of hydrous melt, produced by low-degree partial melting of the less-depleted deeper mantle in a back-arc setting, with the first stage MOR-type partial melting residue may explain this Ti enrichment in the Cr-spl and the crystallization of amphibole in our samples. The high Ti content of cpx in these samples also supports this idea (Fig. 4b). However, the cpx-poor harzburgite samples contain Cr-spl with higher Cr# (57–75), and some of them also show unexpectedly high TiO_2 contents contradicting with their highly depleted nature. Interaction of Ti-poor and Ti-rich boninitic melts, produced by high-degree melting of a formerly-depleted MOR-type mantle in a forearc setting may explain the formation of the highly depleted mantle residues and the high Ti Cr-spl in some of these samples (Fig. 11).

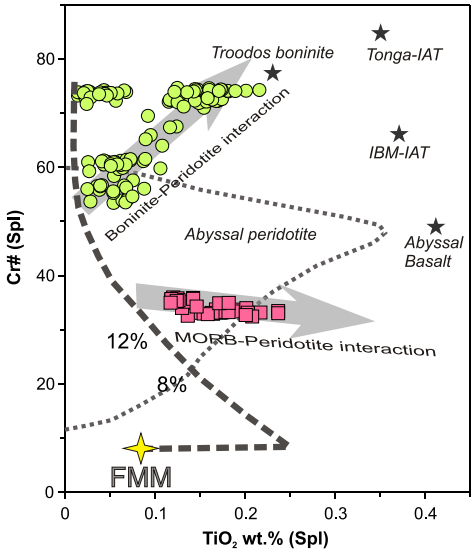

Fig. 11. Compositional variations of Cr# versus TiO_2 (wt.%) content of the Cr-spl (Pearce et al., 2000) in the Refahiye peridotite samples.

7.4.2. Evidence from highly siderophile elements (HSE)

During partial melting of the upper mantle, the Ir-group platinum group elements (IPGE: Os, Ir, Ru) show a compatible behavior and tend to fractionate within the mantle residue, whereas the Pd-group platinum group elements (PPGE: Rh, Pt, Pd) preferentially fractionate within the silicate melt due to their incompatible nature (e.g., Brenan et al., 2003; O'Neill, et al., 2007). The concentrations of the PPGE in the upper mantle peridotites are mainly governed by base metal sulfides (Brenan et al., 2003; Bockrath et al., 2004; Luguet et al., 2007). In upper mantle peridotites, IPGE are preferentially accommodated by more refractory monosulfide solid solutions, whereas the PPGE tend to be controlled by the low-melting point of Cu–Ni-sulfides (e.g., Bockrath et al., 2004). Therefore, melting in the upper mantle at lower temperatures results in the removal of Cu–Ni sulfides as they have lower degrees of melting point than those of monosulfide solid solutions (Bockrath et al., 2004; Luguet et al., 2007). This preferential removal of PPGE and Re carrying the Cu–Ni sulfides causes significant depletion of these elements in the mantle residue. Therefore, IPGE are expected to be enriched compared to PPGE because the IPGE carrier monosulfide solid solutions survive low-degree melting.

In the Refahiye ophiolite, the cpx-rich harzburgite samples (REF13 and REF30), which are represented by low Cr# Cr-spl and high bulk Al_2O_3 contents, are interpreted as the residues of lower degrees of melting compared to the cpx-poor harzburgite samples. These samples are represented by almost flat mantle normalized HSE abundances from Os to Re (Fig. 8) and contradict the above explanation. Their IPGE concentration is slightly enriched compared to the primitive mantle, consistent with their highly compatible nature. However, the lack of PPGE depletion requires the addition of PPGE to the low-degree melting residues (cpx-rich harzburgites) since these elements become depleted in the low-degree partial melting residue. As discussed earlier, the cpx-rich harzburgites contain interstitial cpx and amphibole that we consider as the manifestation of melt impregnation. The inferred melt was likely derived from the more fertile part of the deeper mantle. Percolation of the very low-degrees of partial melt that is enriched in PPGE through the overlying, slightly depleted mantle causes metasomatization and enrichment of the mantle in PPGE and Re.

The mantle-normalized HSE distribution in the cpx-free harzburgite (REF50) is represented with nearly similar IPGE concentrations as in the cpx-rich harzburgite samples, with slight Ir depletion (Fig. 8). However, its PPGE concentration is distinctly lower than those of the cpx-rich harzburgite samples, although its Re contents show an enrichment almost similar to the Re contents of the cpx-rich harzburgites. We infer

that during the first-stage low-degree partial melting of the primitive mantle, most of the low-melting point Cu–Ni sulfides were removed from the upper mantle, resulting in the depletion of PPGE in the residue. After the initiation of subduction in the residual mantle, extensive melting seems to have occurred in the mantle wedge, especially beneath the forearc setting, as a result of fluxing of the upper mantle peridotites by slab-derived hydrous fluids. This melting event might have dissolved the remainder of the Cu–Ni sulfides from the low-degree melting residue and have left behind a highly PPGE-depleted mantle, as evidenced by the occurrence of the mantle-normalized HSE distribution of the cpx-free harzburgite sample (REF50). The Os and Ru contents of this cpx-free harzburgite sample, which contains Cr-spl with Cr# of 75, plot slightly above the mantle values, similar to the cpx-rich harzburgite samples. These observations suggest that the residual sulfide or alloy phases carrying these elements survived the higher-degrees of melting. The depletion of Ir with respect to Os and Ru implies that iridium-bearing sulfides or alloys were progressively consumed during the high-degree partial melting. The Re contents that are higher than the primitive mantle values are not consistent with the highly depleted nature of this sample, indicating that the Re abundance has been disturbed by other processes rather than partial melting. This high concentration of Re content of the highly depleted sample may be explained by Re addition from the subducted slab into the mantle wedge.

7.4.3. Re–Os isotope evidence

During partial melting of the upper mantle, Re prefers to be partitioned into the silicate melt due to its mildly incompatible nature, whereas Os is retained by the residue because of its much higher compatibility compared to Re, resulting in distinct Re/Os ratios for the residual peridotites and the mantle-derived melts (Allegre and Luck, 1980). The lower Re/Os ratios of the upper mantle residues reduce the production of the radiogenic ^{187}Os with time. However, the Re/Os ratios of the mantle-derived melts would be expected to be greatly elevated, causing crustal materials to rapidly accumulate radiogenic ^{187}Os. With time, the Re/Os fractionation that is characteristic of partial melting results in low $^{187}Os/^{188}Os$ ratios for peridotites and high $^{187}Os/^{188}Os$ ratios for mafic rocks of the crustal section of the ophiolites, with almost no overlap between these two rock types (Hauri, 2002).

As the elements Re, Yb and Al behave in a moderately incompatible fashion during partial melting, the concentrations of these elements in the partial melting residue of the upper mantle are expected to correlate with each other (Zheng et al., 2009). On a bivariation diagram, the Yb content of our peridotite and isotropic gabbro samples from the Refahiye ophiolite are well correlated with Al_2O_3, as the Yb content of the upper mantle peridotites plot below the PM value (Fig. 12a). However, the Re content of these samples does not show any correlation with Al_2O_3, and all three peridotite samples plot above the PM value indicating that they are not a simple partial melting residue (Fig. 12b). This scatter in the Re versus Al_2O_3 diagram suggests post-magmatic Re addition, subsequent to the last partial melting event during the MOR or SSZ melt evolution processes. One of the isotropic gabbro samples (REF1) has a similar Yb (0.39 ppm) content to and a lower Re content (0.255 ppb) than the PM, indicating Re loss during the post-magmatic processes (Fig. 12).

The presence of the interstitial amphibole and cpx phases within the cpx-rich harzburgite samples suggests that these rocks were metasomatized by hydrous melts in a SSZ environment. Addition of basaltic component (Al and Ca) and sulfides to the previously depleted mantle peridotites is inevitable during the refertilization process. The addition of sulfides to the previously depleted upper mantle would result in the increase of the original concentration of Re because the Cu–Ni sulfides are the carrier of incompatible HSE and Re (Luguet et al., 2007 and references therein).

The cpx-rich harzburgite samples have higher $^{187}Os/^{188}Os$ ratios (0.12389–0.12400) and lower $^{187}Re/^{188}Os$ (0.28–0.31) ratios compared to the highly depleted harzburgite sample, REF50. However, the Os

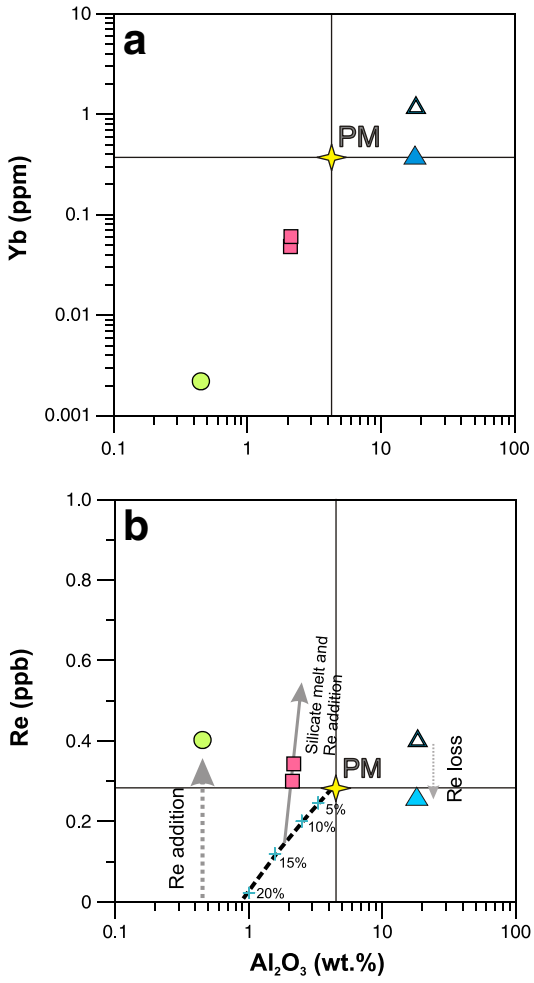

Fig. 12. Covariations of whole-rock Al_2O_3 (wt.%) versus (a) Yb (ppm) and (b) Re (ppb) in the Refahiye ophiolite samples.

isotopic compositions of these samples are lower than the mean present day chondritic value (0.1270; Walker and Morgan, 1989) and the primitive upper mantle (PUM) estimate (0.1296; Meisel et al., 2001), and are represented by sub-chondritic γOs values (−2.36 and −2.44) indicating unradiogenic compositions. The sub-chondritic Os isotopic ratios of the samples with low $^{187}Re/^{188}Os$ ratios suggest a long-term differentiation of the mantle. However, the Re abundances, which are slightly higher than the primitive mantle value, suggest Re addition to the system in some stages of the mantle evolution, either in a MOR or a SSZ environment. Interaction of resulting basaltic melts, produced by low-degree melting of the deeper parts of the mantle at a MOR setting, may increase the Re concentration of the residue and may hence produce supra-chondritic $^{187}Os/^{188}Os$ ratios with time. Nevertheless, the sub-chondritic Os isotopic composition of the cpx-rich harzburgites of the Refahiye ophiolite cannot be explained simply by Re addition during the melting and refertilization processes in a MOR setting.

The low Ti and V contents of the 183 Ma isotropic gabbro sample (REF1) suggest its crystallization from IAT-like melts; however, its low Th/Yb ratio implies that there was no significant incorporation of slab-derived components during the SSZ melt evolution. Trench-distal back-arc basin environments are suitable to produce such types of melts (Dilek and Furnes, 2011), and therefore we infer that the melt, from which this isotropic gabbro crystallized, was produced in a back-arc basin setting. This inferred BAB melt was responsible for the metasomatism and refertilization of the cpx-rich peridotites in the Refahiye ophiolite. The addition of Re during the percolation of BAB-type melt through the overlying mantle is considered to have no significant effect

on the Os isotopic composition of the cpx-rich harzburgites since the addition of Re to the previously depleted MOR mantle occurred geologically recently (183 Ma). Therefore, we suggest that the Re contents of the analyzed samples that are higher than the PM values should be linked to the melting and interaction processes in a trench-distal BAB setting during the closure of Neotethys.

In contrast, the depleted peridotite sample, REF50, is represented by a highly unradiogenic $^{187}Os/^{188}Os$ value of 0.11960, indicating a melt extraction from the mantle that had already been previously depleted. Very high Re abundance (0.39 ppb) and $^{187}Re/^{188}Os$ ratio (0.36) accompanied by a highly depleted nature and the low Os isotopic ratio may reflect the addition of Re also during the SSZ type melt percolation through the mantle.

8. Numerical modeling of partial melting and refertilization events

We have modeled the possible partial melting and refertilization processes that were responsible for the geochemical features of the upper mantle peridotites in the Refahiye ophiolite. The peridotite samples with large Ce anomalies (Ce/Ce* ratios higher than 1.1 and lower than 0.9) are considered as affected from post-magmatic alteration (e.g., Polat et al., 2002). Samples REF13 and REF30 of the cpx-rich harzburgites have Ce/Ce* ratios of 1.04 and 1.24, respectively, indicating that the REE abundances of sample REF30 were slightly altered by secondary processes. The Ce/Ce* ratios of the cpx-poor harzburgites are in the range of 1.76–2.60 indicating that their mobile elements were affected variably by the secondary processes. Therefore, while we discuss the results of the melting models by using the trace and REE abundances, we also take into consideration the other parameters such as the mineral chemistry. Using the partial melting trend proposed by Niu (1997), based on the MgO and Al_2O_3 contents of peridotites, we conclude that the cpx-rich harzburgites are the products of ~12% partial melting whereas the cpx-poor harzburgites are the products of ~25–30% partial melting (Fig. 13a).

The Ni/Yb ratios of the cpx-rich harzburgites are plotted against their Yb contents in Fig. 13b. In this diagram, an open-system dynamic melting (OSDM; Ozawa and Shimizu, 1995; Zou, 1998) model of the primitive mantle (PM, Palme and O'Neill, 2004) is also shown, but this model is independent of fluxing material as these elements are fluid immobile and are also compatible in the mineral phases of the mantle rocks. It is commonly assumed that melting in a MOR setting is generally associated with interaction of the resulting melts derived from the less-depleted deeper mantle. In this respect, we consider an influx of ~1.5% partial melt from the less-depleted (~6%) deeper mantle into the PM source (with a ratio of 2%), which is depleted with a ratio of 10% using the OSDM model (Table 4). This type of melting is referred to as MOR-type melting (Niu, 1997). In the following models we use the 10% depleted mantle as a starting composition.

The presence of the interstitial amphibole in the cpx-rich harzburgites indicates that these rocks were interacted with hydrous melts in a supra-subduction zone (SSZ) environment. We show the OSDM model of the already 10% depleted mantle source in Fig. 13b, whereby a subduction zone component (SZC) is used as a fluxing material (compiled from Eiler et al., 2000, 2007) with a fluxing ratio of 4%. The ~2–4% partial melting of the already 10% depleted mantle can explain the Ni/Yb versus Yb of the cpx-rich harzburgites. These elements are independent of the presence of fluxing material and the fluxing ratio, and they reflect mainly the degree of partial melting. Therefore, we use in

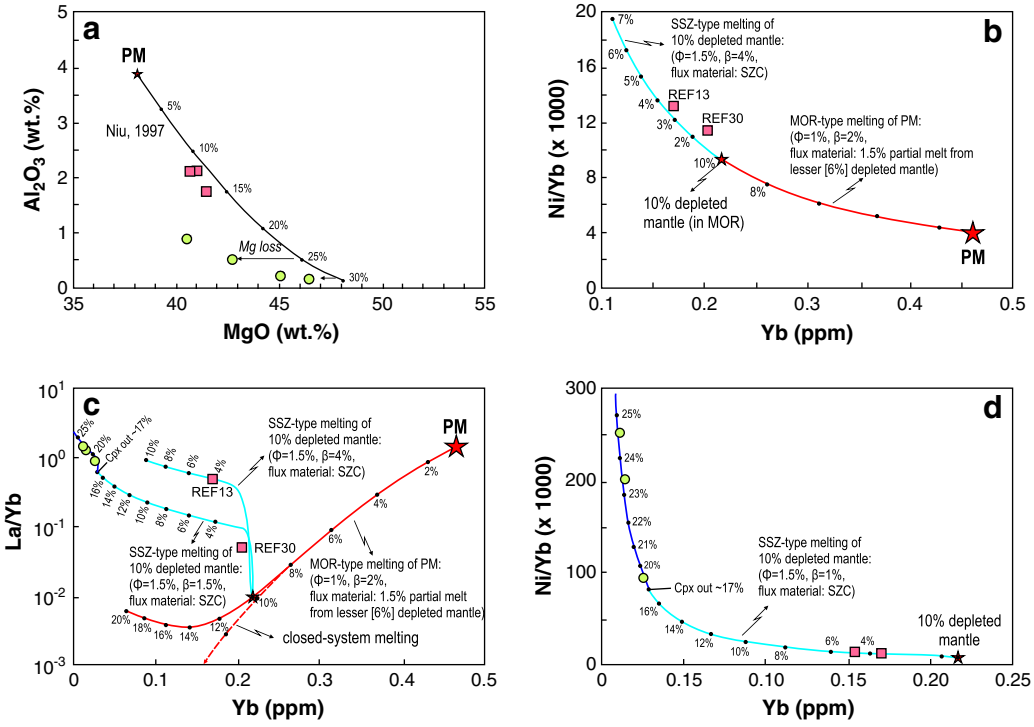

Fig. 13. Numerical melting models for the Refahiye peridotites. (a) Whole rock Al_2O_3 (wt.%) versus MgO (wt.%) diagram. Also shown is the partial melting trend proposed by Niu (1997). (b) Ni/Yb (x1000) versus Yb (ppm) diagram showing the partial melting trend of Primitive Mantle (PM; Palme and O'Neill, 2004) source. On this diagram, the first-stage MOR-type melting is represented by 10% open-system non-modal dynamic melting of PM, during which low-degree (1.5%) partial melt from a 6% depleted deeper mantle section is fluxed (red trajectory). In this model critical melt porosity (Φ) is assumed 1% and mass flux rate (β) is 2% (mass flux rate is the influxing mass fraction – relative to the initial solid – divided by the degree of melting). (c) La/Yb versus Yb (ppm) diagram showing the effects of an open-system over an open-system dynamic melting model. Second-stage SSZ-type melting (blue trajectories) uses 10% depleted mantle as the starting material composition, obtained from the model shown in (b). Two melting trajectories assume Φ = 1.5 and β = 1.5% and 4%. Fluxing material in these models is subduction zone component (SZC; Eiler et al., 2000, 2007). (d) Ni/Yb (×1000) versus Yb (ppm) diagram showing the second-stage partial melting models in (c). Mineral modes: $ol_{0.53(-0.06)} + opx_{0.27(0.28)} + cpx_{0.17(0.67)} + sp_{0.03(0.11)}$ (Kinzler, 1997) for melting of PM during the first stage, and $ol_{0.60(-0.06)} + opx_{0.27(0.28)} + cpx_{0.11(0.67)} + sp_{0.02(0.11)}$ for melting of 10% depleted mantle during the second stage. Cpx is exhausted after ~17% melting during the second-stage. The mineral modes used after this point: $ol_{0.74\ (-0.27)} + opx_{0.26(1.27)}$. Partition coefficients are compiled from McKenzie and OxNions (1991); Suhr (1999); Adam and Green (2006). The numerical results and the parameters are given in Table 4.

Table 4
Melting model parameters used on Fig. 13.

	Partition coefficients				C_0-1 (PM)	6% depleted PM	C_A-1 (1.5% partial melt from 6% depleted mantle)	C_0-2 (10% depleted mantle (fluxed by C_A-1)	C_A-2 (SSZ)
	Olv	Opx	Cpx	Spl					
La	0.000	0.001	0.039	0.001	0.686	0.030	1.538	0.002	112
Yb	0.030	0.077	0.470	0.005	0.462	0.313	2.503	0.217	1
Ni	12.0	3.0	3.0	10.0	1860.0	1946.4	244.8	2022.3	0

Fig. 13c the element La, which is highly incompatible and fluid-mobile. In this way, we can assume that the cpx-rich harzburgites were formed by 12–14% melting of the primitive mantle source in a MOR setting. However, these cpx-rich harzburgites were also affected by metasomatic events in a SSZ setting, refertilizing their medium to heavy REE compositions. Furthermore, considering their higher Cr-spl Cr# with respect to their equivalent rocks from Muğla in SW Turkey, we conclude that the cpx-rich harzburgites might have formed by higher degrees of melting than 12–14%; the subsequent refertilization events must have increased their REE geochemistry. The La/Yb ratio is highly sensitive to the presence of fluxing material during OSDM and to the fluxing ratio, and hence it reflects the effects of any metasomatic processes causing enrichment in light REE concentrations. By using subduction zone component as a fluxing material, with a fluxing ratio of 4%, we conclude that nearly 4% OSDM of an already 10% depleted mantle can account for the La/Yb ratios of sample REF13.

In a similar way, we can explain the Ni/Yb ratios versus Yb contents of the cpx-poor harzburgites with nearly 19–25% OSDM of the 10% depleted mantle with the fluxing rates lower ($\beta = 1.5\%$) than in the previous models (Fig. 13d). We have also modeled this process in Fig. 13c, which explains effectively the La/Yb versus Yb systematics of the depleted rocks. However, considering the disturbed light REE abundances of these rocks, we note that our modeling can only provide an approximation rather than concrete results.

9. Synthesis and summary

The cpx-rich harzburgite samples from the Refahiye ophiolite show great similarities to those upper mantle residues left after low-degree melt extraction at a MOR setting in terms of their whole-rock, high opx (~30%; Kinzler, 1997), and Al_2O_3 and CaO contents. However, the Cr#s (33–38) of Cr-spl from these samples reflect slightly higher degrees of partial melting, and therefore they differ from what the whole-rock Al_2O_3 and CaO contents suggest. Given the higher Cr# values of their Cr-spl, these samples are expected to be more depleted in terms of their cpx content (ol: 68, opx: 28, cpx: 3, spl: 1) (Fig. 14a, A1). In addition, the Cr-spl compositions in these samples represent 14–18% partial melting degree (Fig. 14a, A2). The modeled REE patterns of the 14% and 18% depleted mantle are given in Fig. 14a, A3. In this diagram, the 14% and 18% depleted mantle interacts with the ascending, newly formed fertile melt with a slight enrichment of the LREE contents (auto-fertilization in a MOR environment). In contrast, the REE patterns (Fig. 14a, A3), modeled for the given partial melting degrees (14% and 18%) calculated from the Cr-spl Cr# values, coincide with the PM-normalized REE patterns plotted together with the data obtained from the actual geochemical analysis of the samples. The REE patterns of the cpx-rich peridotite samples (REF13 and REF30) plot slightly above the modeled REE patterns of the given melting degrees. In this respect, the cpx-rich harzburgite samples represent not only the simple partial melting residues, but they also show the evidence for post-magmatic melt interaction and related metasomatism. The occurrence of cpx and amphibole crystals as interstitial phases also supports this inference.

The mafic rock samples show MORB to IAT-like geochemical similarities (Figs. 7, 10b) and are considered to have formed from SSZ-type melt(s). The zircon grains that we separated from the isotropic gabbro sample (REF1) have homogeneous morphological features and display a concordant U–Pb zircon age without older inherited cores. Therefore, we interpret the ^{238}U–^{206}Pb age of 183 Ma of sample REF1 as the crystallization age of the isotropic gabbros, and hence as the timing of the SSZ oceanic crust formation in the Northern Neotethys.

In back arc regions, the degree of melting is relatively low due to the small amount of H_2O, fluids and sediments transported from the subducted slab to the overlying mantle (Kelley et al., 2006; Furnes et al., 2012). Hence, the low-degree melting of a less-depleted, deeper part of the mantle would generate low-volumes of Ti, MREE, LREE and Re-rich melt. During the percolation of this melt through the overlying mantle at shallow depths, cpx and amphibole may precipitate, while secondary ol crystallize along the grain boundaries in the most depleted peridotites (Fig. 14b, D). The interaction of the Ti, MREE, LREE and Re-rich melt with the overlying 14–18% depleted, first stage melting residue, as well as the crystallization of interstitial cpx and amphibole out of this melt, would result in the refertilization of the mantle, and would also increase the REE and some incompatible element (e.g., Ti and Re) contents in the residual peridotites (refertilized samples REF13 and REF30). Therefore, the whole-rock REE and Al_2O_3 contents of these samples reflect lower-degrees of partial melting than those calculated from the Cr# of their Cr-spl phases.

The second stage re-melting of the most depleted (up to ~15%), shallowest part of the lithospheric mantle (first stage MOR-type melting residue) would form a higher-degree depleted mantle residue. Most of the cpx, opx (±ol) available after the first stage melting episode would become consumed during this second stage melting episode, leaving behind highly depleted mantle peridotites (Fig. 14b, B1 and C1). The second stage melting of the already depleted mantle would generate island arc tholeiite to boninitic melts enriched in light REE (due to the contribution from the subducting slab). These melts would be either Ti-poor (Fig. 14b, B) or Ti-richer (Fig. 14b, C) depending on the melting of a more depleted shallower or a less depleted deeper part of the lithospheric mantle, respectively. Interaction of these newly generated SSZ melts with the overlying mantle may result in the equilibration of the mantle mineral phases in the first stage melting residue. During the percolation of this melt, interstitial crystallization of cpx and Cr-spl may also occur (Fig. 14b, B1 and C1). The amount of transported H_2O and LREE from the subducting slab into the mantle wedge at localities B and C in Fig. 14b are expected to be high. The high amount of H_2O addition to the mantle wedge triggers a higher degree of melting (up to 40%, Fig. 14b, B2 and C2), producing melt with high melt/rock ratios. In this case, the generated melt would rise and form an IAT to boninite-like oceanic crust (gabbros and basalts), and would leave behind a highly depleted refractory mantle. The HREE concentrations of these mantle residues decrease as the degree of melting increases. However, these peridotites commonly reflect enriched LREE patterns on PM-normalized diagrams (Fig. 14b, B3 and C3) due to the equilibration of the overlying first-stage depleted mantle residue with light REE-enriched, SSZ type melts.

10. Conclusions

The upper mantle section of the Refahiye ophiolite in NE Turkey contains both cpx-rich and cpx-poor harzburgites. Although the whole-rock and mineral chemical data indicate the formation of the cpx-rich and cpx-poor harzburgites at MOR and SSZ tectonic settings (respectively),

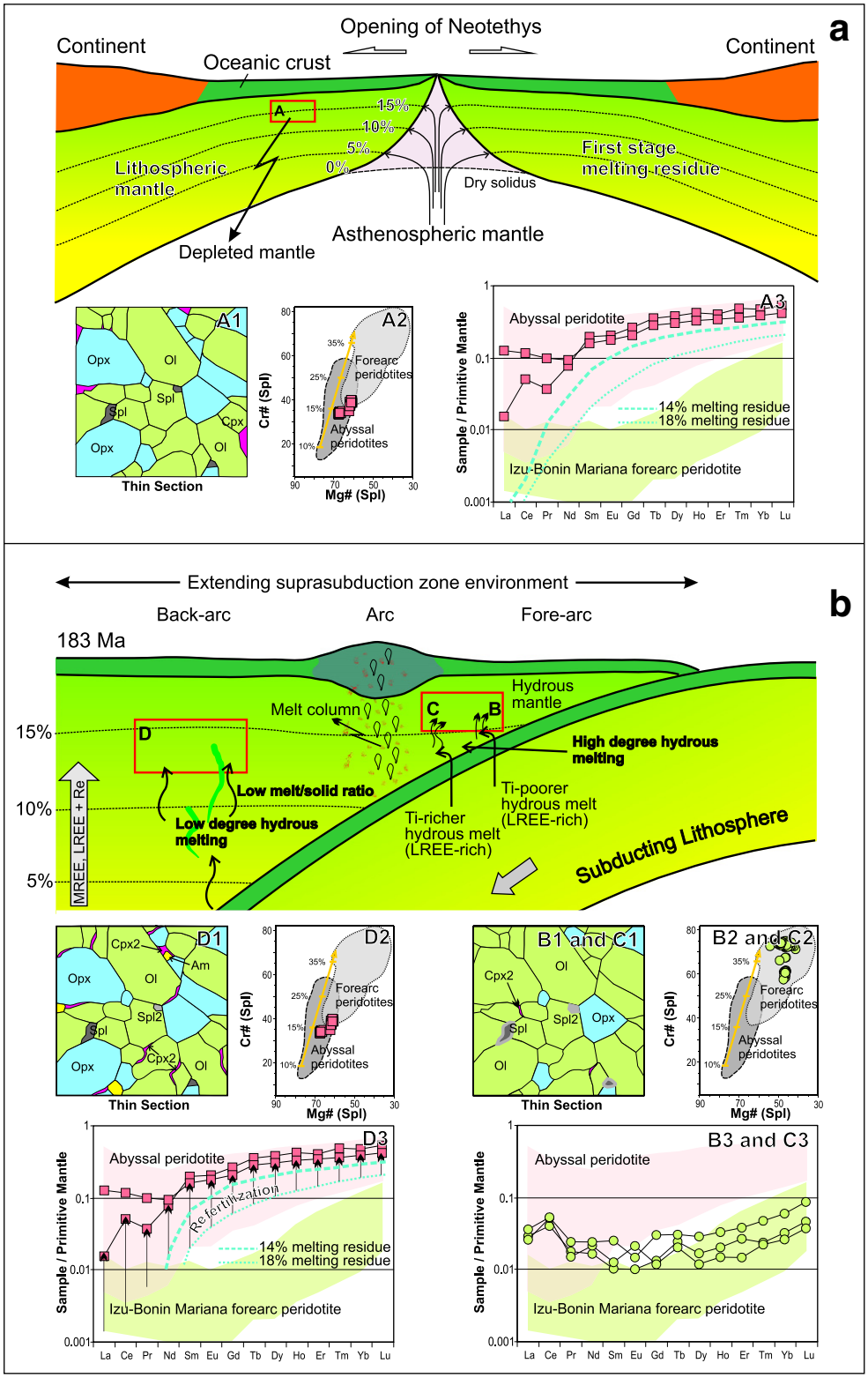

Fig. 14. Tectonic diagram depicting the inferred relative positions of the analyzed samples and the petrogenetic processes involved in their formation relative to MOR (a) and SSZ (b) tectonic settings. See the text under Synthesis and summary for further explanations.

the presence of interstitial cpx and amphibole in the cpx-rich harzburgites points to refertilization of a MOR type mantle by percolating hydrous melts, possibly in a BAB tectonic setting. The highly depleted geochemical signatures of the cpx-poor harzburgites are consistent with their formation in a forearc tectonic environment. The U–Pb zircon age of 183 Ma, obtained from an isotropic gabbro sample in the Refahiye ophiolite, reflects the timing of the SSZ type oceanic crust generation in the Northern Neotethys as the early Jurassic.

Supplementary data to this article can be found online at http://dx.doi.org/10.1016/j.gr.2013.09.008.

Acknowledgements

Our work in the Tethyan ophiolites in Anatolia and beyond has been supported by research grants from the TUBITAK (Turkey), NSF (USA), NATO Science Programme, and Miami University that we gratefully acknowledge. A. Dokuz and F. Aydin are thanked for their help during the field studies and microscopic investigations, respectively. We also thank M. Kaliwoda, K.T. Fehr, R. Hochleitner and D. Müller for their great help with the electron microprobe measurements. S. Arai and T. Morishita provided insightful comments on an earlier version of this manuscript that helped us greatly with our interpretations. We thank A. Polat and the anonymous referee for their constructive and thorough reviews for the Journal that helped us improved the paper.

References

Adam, J., Green, T., 2006. Trace element partitioning between mica- and amphibole-bearing garnet cpx-harzburgite and hydrous basanitic melt: 1. Experimental results and the investigation of controls on partitioning behavior. Contributions to Mineralogy and Petrology 152, 1–17.

Aktimur, H.T., Sarıaslan, M., Keçer, M., Turşucu, A., Ölçer, S., Yurdakul, M.E., Mutlu, G., Aktimur, S., Yıldırım, T., 1995. Geology of Erzincan surrounding. Mineral Research and Exploration Institute (MTA) of Turkey Report no. 9792. (unpublished, in Turkish).

Allegre, C.J., Luck, J.M., 1980. Osmium isotopes as petrogenetic and geological tracers. Earth and Planetary Science Letters 48, 148–154.

Arai, S., 1992. Chemistry of chromian spinel in volcanic rocks as a potential guide to magma chemistry. Mineralogical Magazine 56, 173–184.

Arai, S., 1994. Characterization of spinel peridotites by olivine-spinel compositional relationships, review and interpretation. Chemical Geology 113, 191–204.

Arai, S., Ishimaru, S., 2008. Insights into petrological characteristics of the lithosphere of mantle wedge beneath arcs through peridotite xenoliths: a review. Journal of Petrology 49, 665–695.

Barth, M.G., Gluhak, T.M., 2009. Geochemistry and tectonic setting of mafic rocks from the Othris ophiolite, Greece. Contributions to Mineralogy and Petrology 157, 23–40.

Batanova, V.G., Brügmann, G.E., Bazylev, B.A., Sobolev, A.V., Kamenetsky, V.S., Hofmann, A.W., 2008. Platinum-group element abundances and Os isotope composition of mantle peridotites from the Mamonia complex, Cyprus. Chemical Geology 248, 195–212.

Bédard, É., Hébert, R., Guilmette, C., Lesage, G., Wang, C.S., Dostal, J., 2009. Petrology and geochemistry of the Saga and Sangsang ophiolitic massifs, Yarlung Zangbo Suture Zone, Southern Tibet: evidence for an arc–back-arc origin. Lithos 113, 48–67.

Bockrath, C., Ballhaus, C., Holzheid, A., 2004. Stabilities of laurite RuS_2 and monosulfide liquid solution at magmatic temperature. Chemical Geology 208, 265–271.

Borghini, G., Rampone, E., Crispini, L., De Ferrari, R., Godard, M., 2007. Origin and emplacement of ultramafic–mafic intrusions in the Erro–Tobbio mantle peridotites (Ligurian Alps, Italy). Lithos 94, 210–229.

Brenan, J.M., McDonough, W.F., Dalpe, C., 2003. Experimental constraints on the partitioning of rhenium and some platinum-group elements between olivine and silicate melt. Earth and Planetary Science Letters 212, 135–150.

Choi, S.H., Shervais, J.V., Mukasa, S.B., 2008. Supra–subduction and abyssal mantle peridotites of the Coast Range ophiolite. Contributions to Mineralogy and Petrology 156, 551–576.

Coltorti, M., Bonadiman, C., Faccini, B., Grégoire, M., O'Reilly, S.Y., Powell, W., 2007. Amphiboles from suprasubduction and intraplate lithospheric mantle. Lithos 99, 68–84.

Delavari, M., Amini, S., Saccani, E., Beccaluva, L., 2009. Geochemistry and petrogenesis of mantle peridotites from the Nehbandan Ophiolitic Complex, Eastern Iran. Journal of Applied Sciences 9, 2671–2687.

Dick, H.J.B., Bullen, T., 1984. Chromium spinel as a petrogenetic indicator in abyssal and Alpine-type peridotites and spatially associated lavas. Contributions to Mineralogy and Petrology 86, 54–76.

Dijkstra, A.H., Drury, M.R., Vissers, R.L., 2001. Structural petrology of plagioclase peridotites in the West Othris Mountains (Greece): melt impregnation in mantle lithosphere. Journal of Petrology 42, 5–24.

Dilek, Y., 2006. Collision tectonics of the Eastern Mediterranean region: causes and consequences. Geological Society of America, Special Paper 409, 1–13.

Dilek, Y., Eddy, C.A., 1992. The Troodos (Cyprus) and Kizildag (S. Turkey) ophiolites as structural models for slow-spreading ridge segments. Journal of Geology 100, 305–322.

Dilek, Y., Flower, M.F.J., 2003. Arc-trench rollback and forearc accretion: 2. A model template for Ophiolites in Albania, Cyprus, and Oman. In: Dilek, Y., Robinson, P.T. (Eds.), Ophiolites in Earth History. Geological Society (London) Special Publication, 218, pp. 43–68.

Dilek, Y., Furnes, H., 2009. Structure and geochemistry of Tethyan ophiolites and their petrogenesis in subduction rollback systems. Lithos 113, 1–20.

Dilek, Y., Furnes, H., 2011. Ophiolite genesis and global tectonics: geochemical and tectonic fingerprinting of ancient oceanic lithosphere. The Geological Society of America Bulletin 123, 387–411.

Dilek, Y., Morishita, T., 2009. Melt migration and upper mantle evolution during incipient arc construction: Jurassic Eastern Mirdita ophiolite, Albania. Island Arc 18, 551–554.

Dilek, Y., Robinson, P.T., 2003. Ophiolites in Earth History: introduction. Ophiolites in Earth History. Geological Society of London Special Publication, 218, pp. 1–8.

Dilek, Y., Thy, P., 2009. Island arc tholeiite to boninitic melt evolution of the Cretaceous Kizildag (Turkey) ophiolite: model for multi-stage early arc–forearc magmatism in Tethyan subduction factories. Lithos 113, 68–87.

Dilek, Y., Thy, P., Hacker, B., Grundvig, S., 1999. Structure and petrology of Tauride ophiolites and mafic dike intrusions (Turkey): implications for the Neotethyan ocean. Geological Society of America Bulletin 111, 1192–1216. http://dx.doi.org/10.1130/0016-7606(1999)111<1192:SAPOTO>2.3.CO;2.

Dinter, D.A., 1998. Late Cenozoic extension of the Alpine collisional orogen, northeastern Greece: origin of the north Aegean basin. Geological Society of America Bulletin 110, 1208–1230.

Eiler, J.M., Crawford, A., Elliott, T., Farley, K.A., Valley, J.W., Stolper, E.M., 2000. Oxygen isotope geochemistry of oceanic-arc lavas. Journal of Petrology 41, 229–256.

Eiler, J.M., Schiano, P., Valley, J.W., Kita, N.T., Stolper, E.M., 2007. Oxygen-isotope and trace element constraints on the origins of silica-rich melts in the subarc mantle. Geochemistry, Geophysics, Geosystems 8, Q09012.

Elliott, T., Plank, T., Zindler, A., White, W., Bourdon, B., 1997. Element transport from slab to volcanic front at the Mariana arc. Journal of Geophysical Research 102 (B7), 14991–15019.

Fabriès, J., Bodinier, J.L., Dupuy, C., Lorand, J.P., Benkerrou, C., 1989. Evidence for modal metasomatism in the orogenic spinel lherzolite body from Caussou (Northeastern Pyrenees, France). Journal of Petrology 30, 199–228.

Flower, M.F.J., Dilek, Y., 2003. Arc-trench rollback and forearc accretion: 1. A collision-induced mantle flow model for Tethyan ophiolites. Ophiolites in Earth History. Geological Society of London Special Publication, 218, pp. 21–42.

Furnes, H., Dilek, Y., Pedersen, R.B., 2012. Structure, geochemistry, and tectonic evolution of trench-distal backarc oceanic crust in the western Norwegian Caledonides, Solund-Stavfjord ophiolite (Norway). Geological Society of America Bulletin 124, 1027–1047.

Gaetani, G., 2004. The influence of melt structure on trace element partitioning near the peridotite solidus. Contributions to Mineralogy and Petrology 147, 511–527.

Garuti, G., Fershtater, G., Bea, F., Montero, P., Pushkarev, E.V., Zaccarini, F., 1997. Platinum-group elements as petrological indicators in mafic–ultramafic complexes of the central and Southern Urals, preliminary results. Tectonophysics 276, 181–194.

Hauri, E.H., 2002. Osmium isotopes and mantle convection. Philosophical Transactions of the Royal Society of London A360, 2371–2382.

Hebert, R., Bideau, D., Hekinian, R., 1983. Ultramafic and mafic rocks from the Garret transform fault near 13°30′S on the East Pacific Rise: igneous petrology. Earth and Planetary Science Letters 65, 107–125.

Hebert, R., Adamson, A.C., Komor, S.C., 1990. Metamorphic petrology of ODP 109, Hole 670A serpentinized peridotites: serpentinization processes at a slow spreading ridge environment. In: Detrick, R., Honnorez, J., Bryan, W.B., Juteau, T. (Eds.), Proceedings of the ODP, Sci. Results 106/109. College Station, Texas, pp. 103–115.

Hellebrand, E., Snow, J.E., Mühe, R., 2002. Mantle melting beneath Gakkel Ridge (Arctic Ocean): abyssal peridotite spinel compositions. Chemical Geology 182, 227–235.

Hirata, T., Nesbitt, R.W., 1995. U–Pb isotope geochronology of zircons: evaluation of the laser probe inductively coupled plasma-mass spectrometry technique. Geochimica et Cosmochimica Acta 59, 2491–2500.

Iizuka, T., Hirata, T., 2004. Simultaneous determinations of U–Pb age and REE abundances for zircons using ArF excimer laser-ICPMS. Geochemical Journal 38, 229–241.

Ishii, T., Robinson, P.T., Maekawa, H., Fiske, R., 1992. Petrological studies of peridotites from diapiric serpentinite seamounts in the Izu–Ogasawara–Mariana Forearc, Leg 125. In: Fryer, O., Pearce, J.A., Stokking, L.B. vd (Eds.), Proceedings of the Ocean Drilling Program, Scientific Results, 125. Ocean Drilling Program, College Station, TX, pp. 445–485.

Ishimaru, S., Arai, S., Ishida, Y., Shirasaka, M., Okrugin, V.M., 2007. Melting and multi-stage metasomatism in the mantle wedge beneath a frontal arc inferred from highly depleted peridotite xenoliths from the AvachaVolcano, Southern Kamchatka. Journal of Petrology 48, 395–433.

Ishizuka, O., Tani, K., Reagan, M.K., Kanayama, K., Umino, S., Harigane, Y., Sakamoto, I., Miyajima, Y., Yuasa, M., Dunkley, D.J., 2011. The timescales of subduction initiation and subsequent evolution of an oceanic island arc. Earth and Planetary Science Letters 306, 229–240.

Iwano, H., Orihashi, Y., Danhara, T., Hirata, T., Ogasawara, M., 2012. Evaluation of fission-track and U–Pb double dating method for identical zircon grains using homogeneous zircon grains in Kawamoto Granodiorite in Shimane prefecture, Japan. Journal of the Geological Society of Japan 118, 365–375 (in Japanese with English abstract).

Johnson, K.T.M., Dick, H.J.B., Shimizu, N., 1990. Melting in the oceanic upper mantle: an ion microprobe study of diopsides in abyssal peridotites. Journal of Geophysical Research 95, 2661–2678.

Kelley, K.A., Plank, T., Newman, S., Stolper, E., Grove, T.L., Hauri, E., 2006. Mantle melting as a function of water content at subduction zones. I: Back-arc basins. J. Geophysical Research 111, B09208.

Kinzler, R.J., 1997. Melting of mantle peridotite at pressures approaching the spinel to garnet transition: application to mid-ocean ridge basalt petrogenesis. Journal of Geophysical Research 102, 853–874.

Kinzler, R.J., Grove, T.L., 1992. Primary magmas of mid-ocean ridge basalts 1. Experiments and methods. Journal of Geophysical Research 97, 6885–6906.

Langmuir, C.H., Klein, E.M., Plank, T., 1992. Petrological systematics of mid-ocean ridge basalts: constraints on melt generation beneath ocean ridges. In: Morgan, J.P., Blackman, D.K., Sinton, J.M. (Eds.), Mantle Flow and Melt Generation at Mid-Ocean Ridges. Geophysical Monograph. American Geophysical Union, pp. 183–280.

Leake, B.E., Woolley, A.R., Arps, C.E.S., 1997. Nomenclature of amphiboles. Reports of the subcommittee on amphiboles of the International Mineralogical Association Commission on newminerals and mineral names. European Journal of Mineralogy 9, 623–651.

Liu, C.Z., Wu, F.Y., Wilde, S.A., Yu, L.J., Li, J.L., 2010. Anorthitic plagioclase and pargasitic amphibole in mantle peridotites from Yungbwa ophiolite (southern Tibetan Plateau) formed by hydrous melt metasomatism. Lithos 114, 413–422.
Luguet, A., Shirey, S.B., Lorand, J.P., Horan, M.F., Carlson, R.W., 2007. Residual platinum group minerals from highly depleted harzburgites of the Lherz massif (France) and their role in HSE fractionation of the mantle. Geochimica et Cosmochimica Acta 71, 3082–3097.
McDonough, W.F., Sun, S.S., 1995. The composition of the earth. Chemical Geology 120, 223–253.
McKenzie, D., O'Nions, R.K., 1991. Partial melt distributions from inversion of rare Earth element concentrations. Journal of Petrology 32, 1021–1091.
Meisel, T., Moser, J., Fellner, N., Wegscheider, W., Schoenberg, R., 2001. Simplified method for the determination of Ru, Pd, Re, Os, Ir and Pt in chromitites and other geological materials by isotope dilution ICPMS and acid digestion. Analyst 126, 322–328.
Meisel, T., Fellner, N., Moser, J., 2003. A simple procedure for the determination of platinum group elements and rhenium (Ru, Rh, Pd, Re, Os, Ir and Pt) using ID-ICP-MS with an inexpensive on-line matrix separation in geological and environmental materials. Journal of Analytical Atomic Spectrometry 18, 720–726.
Morishita, T., Dilek, Y., Shallo, M., Tamura, A., Arai, S., 2011. Insight into the uppermost mantle section of a maturing arc: the Eastern Mirdita ophiolite, Albania. Lithos 124, 215–226.
Niu, Y., 1997. Mantle melting and melt extraction processes beneath ocean ridges: evidence from abyssal peridotites. Journal of Petrology 38, 1047–1074.
Niu, Y., 2004. Bulk-rock major and trace element compositions of abyssal peridotites: implications for mantle melting, melt extraction and post-melting processes beneath mid ocean ridges. Journal of Petrology 45, 2423–2458.
O'Neill, C., Lenardic, A., Jellinek, A.M., Kiefer, W.S., 2007. Melt propagation and volcanism in mantle convection simulations, with applications for Martian volcanic and atmospheric evolution. Journal of Geophysical Research 112, E07003.
Okay, A.I., 1984. Metamorphic belts in Northwest Anatolia. Ketin Symposium Proceedings 83–92 (in Turkish with English abstract).
Okay, A.I., Monod, O., Monié, P., 2002. Triassic blueschists and eclogites from northwest Turkey: vestiges of the Paleo-Tethyan subduction. Lithos 64, 155–178.
Ottley, C.J., Pearson, D.G., Irvine, G.J., 2003. A routine method for the dissolution of geological samples for the analysis of REE and trace elements via ICP-MS. In: Holland, J.G., Taner, S.D. (Eds.), Plasma Source Mass Spectrometry, Applications and Emerging Technologies. The Royal Society of Chemistry, pp. 221–230.
Ozawa, K., Shimizu, N., 1995. Open-system melting in the upper mantle: constraints from the Hayachine–Miyamori ophiolite, northeastern Japan. Journal of Geophysical Researches 100, 22315–22335.
Özen, H., Çolakoğlu, A.O., Sayak, H., Dönmez, C., Türkel, A., Odabaşı, I., 2008. Report of Cr-Ni prospection and ophiolite geology of Erzincan-Tercan-Çayırlı region. General Directorate of Mineral Research and Exploration, Report No: 11055 (In Turkish).
Özgül, N., 1981. Geology of Munzur Mountains. Mineral Research and Exploration Institute of Turkey (MTA) Report no. 6995. (unpublished, in Turkish).
Paliulionyte, V., Meisel, T., Ramminger, P., Kettisch, P., 2006. High pressure asher digestion and an isotope dilution-ICP-MS method for the determination of platinum-group element concentrations in chromitite reference materials CHR-Bkg, GAN Pt-1 and HHH. Geostandards and Geoanalytical Research 30, 87–96.
Palme, H., O'Neill, H.St.C., 2004. Cosmochemical estimates of mantle composition. In: Holland, H.D., Turrekian, K.K. (Eds.), Treatise on Geochem., vol 2. Elsevier, Amsterdam, pp. 1–38.
Parkinson, I.J., Pearce, J.A., 1998. Peridotites from the Izu–Bonin–Mariana Forearc (ODP Leg 125), Evidence for mantle melting and melt–mantle interaction in a supra-subduction zone setting. Journal of Petrology 39, 1577–1618.
Parkinson, I.J., Pearce, J.A., Thirlwall, M.F., Johnson, K.T.M., Ingram, G., 1992. Trace element geochemistry of peridotites from the Izu–Bonin–Mariana forearc, Leg 125. In: Fryer, P., Pearce, J.A., Stokking, L.B., et al. (Eds.), Proceedings of the Ocean Drilling Program Scientific Results, 125. Ocean Drilling Program, College Station, TX, pp. 487–506.
Pearce, J.A., 2008. Geochemical fingerprinting of oceanic basalts with applications to ophiolite classification and the search for Archean oceanic crust. Lithos 100, 14–48.
Pearce, J.A., Robinson, P.T., 2010. The Troodos ophiolitic complex probably formed in a subduction initiation, slab edge setting. Gondwana Research 18, 60–81.
Pearce, J.A., Barker, P.F., Edwards, S.J., Parkinson, I.J., Leat, P.T., 2000. Geochemistry and tectonic significance of peridotites from the South Sandwich Arc-basin Systems, South Atlantic. Contributions to Mineralogy and Petrology 139, 36–53.
Piccardo, G.B., Zanetti, A., Müntener, O., 2007. Melt/peridotite interaction in the Southern Lanzo peridotite: field, textural and geochemical evidence. Lithos 94, 181–209.
Polat, A., Hofmann, A.W., Rosing, M.T., 2002. Boninite-like volcanic rocks in the 3.7–3.8 Ga Isua greenstone belt, West Greenland: geochemical evidence for intra-oceanic subduction zone processes in the early Earth. Chemical Geology 184, 231–254.
Pouchou, J.L., Pichoir, F., 1984. A new model for quantitative X-ray microanalysis. Application to the analysis of homogeneous samples. La Recherche Aérospatiale 3, 13–38.
Rampone, E., Piccardo, G.B., Vannucci, R., Bottazzi, P., 1997. Chemistry and origin of trapped melts in ophiolitic peridotites. Geochimica et Cosmochimica Acta 61, 4557–4569.
Rampone, E., Piccardo, G.B., Hofmann, A.W., 2008. Multi-stage melt–rock interaction in the Mt. Maggiore (Corsica, France) ophiolitic peridotites: microstructural and geochemical evidence. Contributions to Mineralogy and Petrology 156, 453–475.
Reagan, M.K., Ishizuka, O., Stern, R.J., Kelley, K.A., Ohara, Y., Blichert-Toft, J., Bloomer, S.H., Cash, J., Fryer, B.B., Hickey-Vargas, R., Ishii, T., Kimura, J.-I., Peate, D.W., Rowe, M.C., Woods, M., 2010. Fore-arc basalts and subduction initiation in the Izu–Bonin–Mariana system. Geochemistry, Geophysics, Geosystems 11, Q03X12.
Rice, S.P., Robertson, A.H.F., Ustaömer, T., 2006. Late Cretaceous-Early Cenozoic tectonic evolution of the Eurasian active margin in the Central and Eastern Pontides, northern Turkey. Geological Society, London, Special Publications 260, 413–445.
Ricou, L.E., 1980. The structural behaviour of Taurus belt between Hellenides and Zagrids. Geological Society of Turkey Bulletin 23, 101–118 (in Turkish with English abstract).
Roux, V.L., Bodinier, J.-L., Tommasi, A., Alard, O., Dautria, J.-M., Vauchez, A., Riches, A.J.V., 2007. The Lherz spinel lherzolite: refertilized rather than pristine mantle. Earth and Planetary Science Letters 259, 599–612.
Saccani, E., Photiades, A., 2004. Mid-ocean ridge and supra-subduction affinities in the Pindos ophiolites (Greece): implications for magma genesis in a forearc setting. Lithos 73, 229–253.
Saccani, E., Beccaluva, L., Photiades, A., Zeda, O., 2011. Petrogenesis and tectono-magmatic significance of basalts and mantle peridotites from the Albanian–Greek ophiolites and sub-ophiolitic mélanges. New constraints for the Triassic–Jurassic evolution of the Neo-Tethys in the Dinaride sector. Lithos 124, 227–242.
Sarifakioglu, E., Özen, H., Winchester, J.A., 2009. Petrogenesis of the Refahiye ophiolite and its tectonic significance for Neotethyan ophiolites along the Izmir–Ankara–Erzincan Suture Zone. Turkish Journal of Earth Sciences 18, 187–207.
Sarifakioglu, E., Dilek, Y., Sevin, M., 2013. Jurassic–Paleogene intra-oceanic magmatic evolution of the Ankara Mélange, North-Central Anatolia, Turkey. Solid Earth (in press).
Saunders, A.D., Norry, M.J., Tarney, J., 1991. Fluid influence on the trace element compositions of subduction zone magmas. Philosophical Transactions of Physical Sciences and Engineering 335, 377–392.
Seyler, M., Toplis, M.J., Lorand, J.P., Luguet, A., Cannat, M., 2001. Cpx microtextures reveal incompletely extracted melts in abyssal peridotites. Geology 29, 155–158.
Seyler, M., Lorand, J.-P., Dick, H.J.B., Drouin, M., 2007. Pervasive melt percolation reactions in ultra-depleted refractory harzburgites at the Mid-Atlantic Ridge, 15°20'N: ODP Hole 1274A. Contributions to Mineralogy and Petrology 153, 303–319.
Shervais, J.W., 1982. Ti–V plots and the petrogenesis of modern and ophiolitic lavas. Earth and Planetary Science Letters 59, 101–118.
Shirey, S.B., Walker, R.J., 1998. Re–Os isotopes in cosmochemistry and high-temperature geochemistry. Annual Review in Earth and Planetary Science 26, 423–500.
Smoliar, M.I., Walker, R.J., Morgan, J.W., 1996. Re-Os ages of group IIA, IIIA, IVA and IVB iron meteorites. Science 271, 1099–1102.
Suhr, G., 1999. Melt migration under oceanic ridges: inferences from reactive transport modelling of upper mantle hosted dunites. Journal of Petrology 40, 575–599.
Ulrich, M., Picard, C., Guillot, S., Chauvel, C., Cluzel, D., Meffre, S., 2010. Multiple melting stages and refertilization as indicators for ridge to subduction formation: the New Caledonia ophiolite. Lithos 115, 223–236.
Uysal, I., Kaliwoda, M., Karslı, O., Tarkian, M., Sadıklar, M.B., Ottley, C.J., 2007. Compositional variations in whole rock and coexisting phases with partial melting and melt–peridotite interaction in an upper mantle section from the Ortaca Area, Southwestern Turkey. Canadian Mineralogist 45, 1471–1493.
Uysal, I., Ersoy, E.Y., Karsli, O., Dilek, Y., Sadiklar, M.B., Ottley, C.J., Tiepolo, M., Meisel, T., 2012. Coexistence of abyssal and ultra-depleted SSZ type mantle peridotites in a Neo-Tethyan Ophiolite in SW Turkey: constraints from mineral composition, whole-rock geochemistry (major–trace–REE–PGE), and Re–Os isotope systematics. Lithos 132–133, 50–69.
Uysal, I., Sen, A.D., Ersoy, E.Y., Dilek, Y., Saka, S., Zaccarini, F., Escayola, M., Karslı, O., 2013. Geochemical make-up of oceanic peridotites from NW Turkey and the multi-stage melting history of the Tethyan upper mantle. Mineralogy and Petrology. http://dx.doi.org/10.1007/s00710-013-0277-3.
Walker, R.J., Morgan, J.W., 1989. Rhenium–osmium isotope systematics of carbonaceous chondrites. Science 243, 519–522.
Wiedenbeck, M., Alle, P., Corfu, F., Griffin, W.L., Meier, M., Oberli, F., Von Quadt, A., Roddick, J.C., Spiegel, W., 1995. Three natural zircon standards for U-Th-Pb, Lu-Hf, trace element and REE analyses. Geostandards Newsletter 19, 1–23.
Witt-Eickschen, G., Harte, B., 1994. Distribution of trace elements between amphibole and clinopyroxene from mantle peridotites of the Eifel (western Germany); an ion-microprobe study. Chemical Geology 117, 235–250.
Yılmaz, A., 1985. Basic geological characteristics and structural evolution of the region between the upper Kelkit Creek and the Munzur Mountains. Geological Society of Turkey Bulletin 28, 79–82.
Yılmaz, A., Terlemez, İ., Uysal, Ş., 1990. Geological characteristics and structural evolution of the ophiolitic units around Sakaltutan Dağ (Erzurum), Turkey. Middle East Technical University of Journal of Pure and Applied Sciences, 21, pp. 221–235.
Yokoyama, T.D., Suzuki, T., Kon, Y., Hirata, T., 2011. Determinations of rare earth element abundance and U–Pb age of zircons using multisport laser ablation-inductively coupled plasma mass spectrometry. Analytical Chemistry 83, 8892–8899.
Zheng, L., Zhi, X., Reisberg, L., 2009. Re–Os systematics of the Raobazhai peridotite massifs from the Dabie orogenic zone, eastern China. Chemical Geology 268, 1–14.
Zou, H.B., 1998. Trace element fractionation during modal and nonmodal dynamic melting and open-system melting: a mathematical treatment. Geochimica et Cosmochimica Acta 62, 1937–1945.